GUILHERME ADINOLFI COLPAERT SARTORI

FATIGUE OF PEARLITIC STEELS USED FOR BRIDGE CABLES

São Paulo

2020

GUILHERME ADINOLFI COLPAERT SARTORI

FATIGUE OF PEARLITIC STEELS USED FOR BRIDGE CABLES

Undergraduate Thesis, Escola Politécnica da Universidade de São Paulo

Area:

Metallurgical Engineering

Supervisors: Prof. Dr. Cesar Roberto de Farias Azevedo and Prof. Dr. Jean-Bernard Vogt

Co-supervisor: Isadora Costa

São Paulo

2020

Cataloguing in publication

Sartori, Guilherme Adinolfi Colpaert
Fatigue of pearlitic steels used for bridge cables / G. A. C Sartori – São Paulo 2020.
63 p.

Undergraduate Thesis – Escola Politécnica da Universidade de São Paulo. Department of Metallurgical and Materials engineering.

1.Fatigue testing 2.Pearlitic steel microstructure 3.SEM 4.Interlamellar spacing 5.Cyclic softening I. University of São Paulo. Department of Metallurgical and Materials Engineering II.t.

Acknowledgement

I would like to thank all the people involved in the realization of this project, in special Prof. Jean-Bernard Vogt and Isadora Costa, who guided, helped and encouraged us during all the process, in a kind and patient manner.

I also would like to thank Ana Clara Amado Dolabella and Ana Beatriz Belletti Lopes Aires for sharing this project with me, always helping in the experiments, giving ideas and suggestions, and analysing the results by my side.

Thanks to Laís Ávila, Mahira Araujo and Arthur Boidot, who realize their thesis in the laboratory, for always keeping a good work environment and for all the advice.

A special thanks also go to Damien Creton and Jocelyn Golek for the help in the use of the machines and the preparation of the specimens.

I would like to acknowledge Prof. Cesar Azevedo for discussing patiently the results obtained during the validation of this project for the final thesis in the University of São Paulo (USP), giving me another vision of the data and generating interesting and meaningful discussions.

Finally, I thank the enterprise Bekaert for the financing of our project and for providing all the samples for our tests and for all the team of the laboratory Unité Matériaux et Transformations, of the University of Lille and the École Nationale Supérieure de Chimie de Lille (ENSCL), for making this study possible.

Abstract

The objective of this study was to analyze the behaviour of pearlitic steels used for bridge cables and evaluate the influence of material interlamellar spacing (fine pearlite, with an interlamellar spacing of 72 nm, and coarse pearlite with an interlamellar space of 143 nm) on fatigue properties, using the strain life approach. The controlled deformation tests were carried out in four different levels of total deformation (0.6%, 0.8%, 1.2% and 1.6%). A cyclic softening was observed for all the samples, together with the phenomenon of relaxation. In fine pearlite, those effects were more drastic. The surfaces of fracture, relief marks and small crack propagation were analyzed using scanning electrons microscopy to a better understanding of the fatigue mechanism. The fracture surface presented always a first stable propagation zone with microplastic tearing, while the final fracture was either by cleavage, for higher deformation levels, or with dimples, for lower deformations. The relief marks agree with the results of the fatigue test. The analysis of small cracks showed that for both coarse and fine pearlite the crack propagates in a transgranular direction.

Keywords: fatigue testing, pearlitic steel microstructure, SEM, interlamellar spacing, cyclic softening.

Resumo

O objetivo deste estudo foi analisar o comportamento de aços perlíticos usados para cabos de pontes e avaliar a influência do espaçamento interlamelar do material (perlita fina, com espaçamento interlamelar de 72 nm, e perlita grossa com espaçamento interlamelar de 143 nm) nas propriedades de fadiga, utilizando a abordagem deformação-vida. Os testes de deformação controlada foram realizados em quatro níveis diferentes de deformação total (0,6%, 0,8%, 1,2% e 1,6%). Foi observado um amolecimento cíclico para todas as amostras, juntamente com o fenômeno de relaxamento. Na perlita fina, esses efeitos foram mais drásticos. As superfícies de fratura, marcas de relevo e propagação de pequenas trincas foram analisadas usando microscopia eletrônica de varredura para um melhor entendimento do mecanismo de fadiga. A superfície de fratura apresentou sempre uma primeira zona de propagação estável com rompimento microplástico, enquanto a fratura final foi por clivagem, para maiores níveis de deformação, ou com alvéolos, para menores deformações. As marcas de relevo estão de acordo com os resultados do teste de fadiga. A análise das pequenas fissuras mostrou que a fissuração inicial na direção transgranular, tanto para perlita fina quando para perlita grossa.

Palavras-chave: teste de fadiga, microestrutura perlítica, espaçamento interlamelar, amolecimento cíclico.

FIGURES LIST

TABLES LIST

Summary

1. Introduction

Steel remains one of the most used civil construction materials due to its relatively low cost and its excellent and adaptable mechanical properties. Changing the heat treatment and the alloying elements of steel makes it possible to control each phase amount and morphology, producing a wide range of mechanical properties. Among the several uses of steel, the present work will focus on bridge cables.

The critic mechanical load on the bridges is due to loaded trucks. Therefore, it is reasonable to assume that the stress imposed on these cables is not constant; they change with the traffic, which constitutes a fatigue-like solicitation. On average, over 1,000 of those vehicles transit each day, producing over 27 million cycles of load and unload in 75 years [1]. This shows how important it is to understand the behaviour of steel in fatigue to construct new bridges or maintenance the old ones.

Among the different microstructures of the steel, one that stands out to produce the helicoidal cable wires is the pearlite. The eutectoid decomposition of the austenite produces the pearlite, which is composed of ferrite-α and cementite (Fe_3C) in a lamellar arrangement [2]. Ferrite is known for being softer and ductile, while cementite is hard and brittle. The combination of both phases in a lamellar microstructure produces a synergism, creating a material both resistant and ductile. There is an interface strengthening between the phases, a solid solution strengthening of supersaturated carbon atoms by cementite decomposition and dislocation strengthening in narrow ferrite regions. Besides, the dislocation structure formed in the interface protects the cementite from cracking in traction and compression [3].

The pearlite was first observed by Sorby [4] in 1864, but due to the lack of theoretical interpretation at the time, it got little attention. Only with the improvement of optical microscopy techniques, Carpenter and Robertson [5] observed the formation of pearlite colonies in 1932. Later, Mehl and Hagel [6], in 1956, detailed the pearlitic microstructure and generated the first measurements of its nucleation and growth rates. The knowledge about the pearlite is growing

until actual days, and its history shows the importance of always combining experimental technics with the study of physical metallurgy.

The pearlitic transformation happens as the steel is cooled down from the austenite phase field because austenite ceases to be thermodynamically stable. The undercooling needs to be enough to create the interface between the phases, that requires energy. The austenite decomposition occurs at about 727 °C for Fe-C binary steels [2, 7]. The mechanism of perlite formation starts with a cementite particle (metastable phase) that nucleates randomly and heterogeneously along the austenite grain boundaries. As cementite presents an amount of carbon higher than the solubility limit of austenite, the adjacent regions will be poorer in carbon, promoting ferrite formation. As this ferrite is formed, the excess carbon atoms will diffuse into the neighbouring areas, enabling the cementite nucleation. The repetition of these events will create a lamellar microstructure, as illustrated in **Figure 1-a** to **1-d.** The perlite nucleation tends to happen heterogeneously on the prior-austenitic grain boundary (PAGB) [2, 7, 8]. That is why the nucleation and growth of pearlite are said to be cooperative.

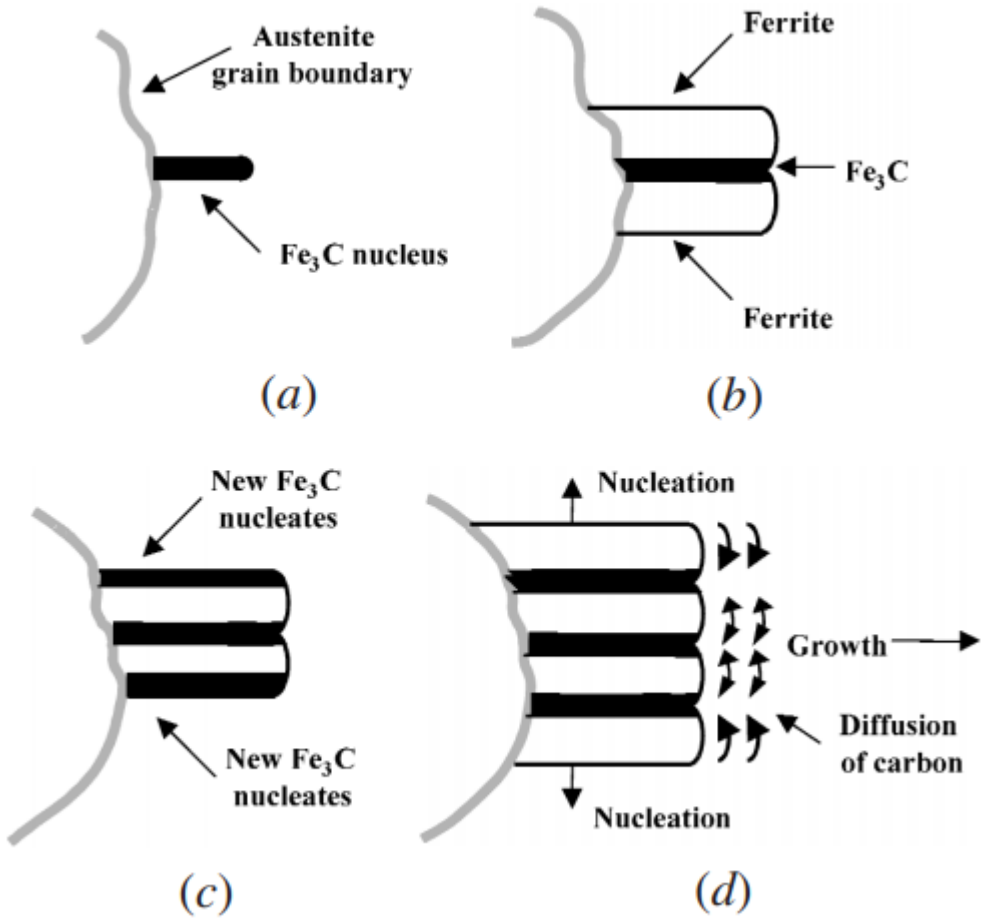

Figure 1 *- Schematic representation of the cooperative nucleation and growth of pearlite with (a) the first nucleation spot of cementite, (b) the nucleation of ferrite nearby due to the reduced amount of carbon in those regions (c) the nucleation of cementite close to the ferrite, due to the local increase in carbon concentration and (d) summarising the entire mechanism of nucleation and growth [5].*

This mechanism depends drastically on carbon diffusion. A higher undercooling from the austenitic decomposition temperature results in a more important driving force for the reaction, but there is a decrease in the carbon diffusion. Therefore, lower transformation temperatures will form finer pearlite lamellas (smaller interlamellar spacing). The nucleation and growth showed in **Figures 1-a** to **1-d** happen in multiples areas along the austenitic grain boundary, creating several regions with different orientations of the lamellas. Each region with the same set of directions for a lamella crystalline structure is called a pearlite colony and each colony has its proper orientation. Besides, new pearlite colonies can nucleate next to existing pearlite colonies [9, 10].

The prior austenitic grain size, the pearlite colony size and the interlamellar spacing mostly describe the mechanical properties of pearlitic steels. The yield

strength is defined principally by the interlamellar spacing, following a Hall-Petch equation [11, 12, 13], expressed in **Equation 1**. Theories explain this model by a dislocation pile-up model for the stress concentration at the tip of a slip band [14, 15]. In pearlitic steels, the interlamellar space is used in the equation due to its effect as a dislocation slip barrier [17].

$$\sigma_y = \sigma_0 + k\lambda^{-1/2} \quad (1)$$

Where:

$\boldsymbol{\sigma_y}$ is the yield strength, $\boldsymbol{\sigma_0}$ is the friction stress for ferrite to dislocation motion, λ is the pearlite interlamellar spacing.

The pearlite interlamellar spacing (λ) also influences the fatigue properties drastically. Fatigue is the progressive, localized, and permanent structural change that occurs in steel subjected to repeated or fluctuating strains at nominal stress that have maximum values usually less than the static yield strength of the material [17]. As fatigue is the typical way an engineering material fails during use [18]; thus, it is essential to understand the mechanics behind fatigue cracking. Usually, fatigue crack nucleates in the surface, in stress concentration points, such as notches, defects, corrosion pits and inclusions. However, in defect-free polished surfaces, intrusion and extrusions topographic marks promote the fatigue crack nucleation. When the stress amplitude is high enough, plastic deformation occurs. This creates slip steps in the surface that accumulate and form intrusions and extrusions in the surface, roughening it and leading to the forming of microcracks. Those microcracks will propagate first by a shear mode, called stage I, where it grows across several grains. Later, the tensile strain range will control the propagation in a zigzag manner, with a steady crack growth rate, in stage II of the Paris-Erdogan crack growth versus the numbers of cycles curve, as in **Figure 2,** that shows the behaviour of two pearlitic steel (R260 in (a) and R370 in (b) with two orientations (LS and LT)). The three more common modes for the stable propagation are by striation formation, microvoid coalescence and microcleavage [18]. When the remaining resistant section is not enough to support the stress, the crack will propagate unstably by brittle (cleavage, rupture, intergranular fracture and transgranular fracture) or ductile fracture [18, 19].

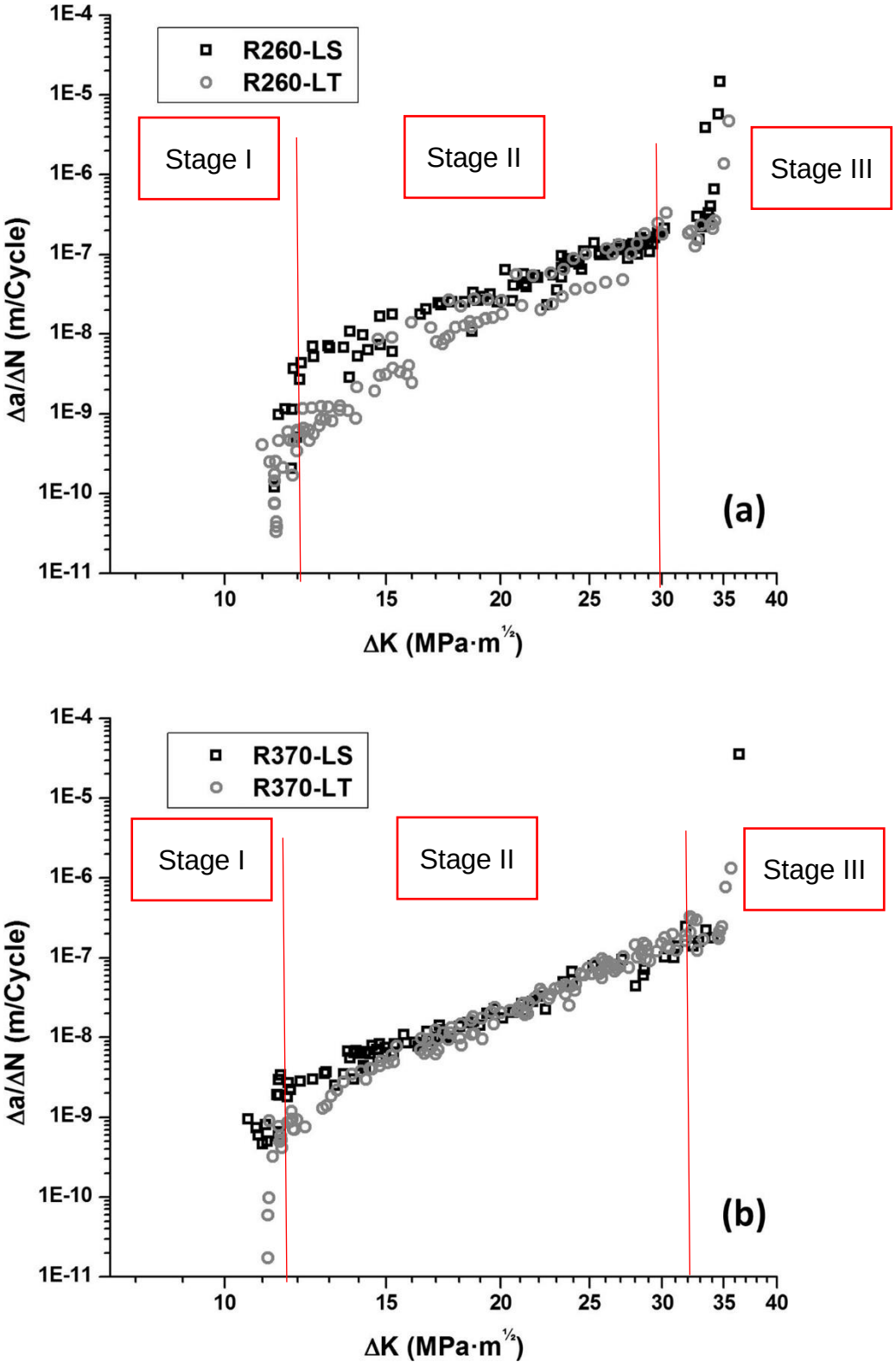

Figure 2 *- Fatigue crack growth rate versus stress intensity range for rail steel grade pearlitic steels [20] of two compositions (R260 in (a) and R370 in (b)) in two orientations. In the graphics, it is possible to see that in the start, the crack grows highly with the stress intensity, in Stage I. Next, it grows with a stable lower rate, in Stage II, and finally, it grows unstably, causing the fracture in Stage III.*

The interest in studying the pearlite for application involving fatigue becomes more evident as we look at the pearlitic microstructure. The cementite, as a more rigid phase, presents itself as an obstacle for the dislocation slip in the ferrite and to the fatigue crack propagation. Therefore, the cementite retards fatigue crack growth. [19, 21]. Different parameters of the pearlitic microstructure may play an essential role in the final fatigue properties, such as the prior austenite grain size, the pearlite colony size, the pearlitic interlamellar spacing and the volumetric fraction of cementite. Gray et al. [22] showed that a decrease in the interlamellar spacing increased the fatigue crack initiation and the fatigue limit, indicating that the interfacial barriers imposed by the cementite phase are more relevant than the prior austenite grain boundaries or the pearlitic colony boundaries for improving the mechanical strength. Ravichandran [16] showed that the fatigue crack growth is strongly dependent on the pearlitic colony size and that fatigue crack propagation can occur across the lamella or along the lamellar direction in the ferrite phase, as shown in **Figures 3-a** and **3-b**. The shear stress controls the fatigue crack growth, and the crack propagates in a zigzag manner caused by crack deflections in the colony boundaries, creating a “rough fracture surface” [19], as shown in **Figures 4-a** to **4-d**. In addition, the development of plastic deformation in the crack tip is inhibited by the presence of pearlite, increasing the fatigue resistance [23].

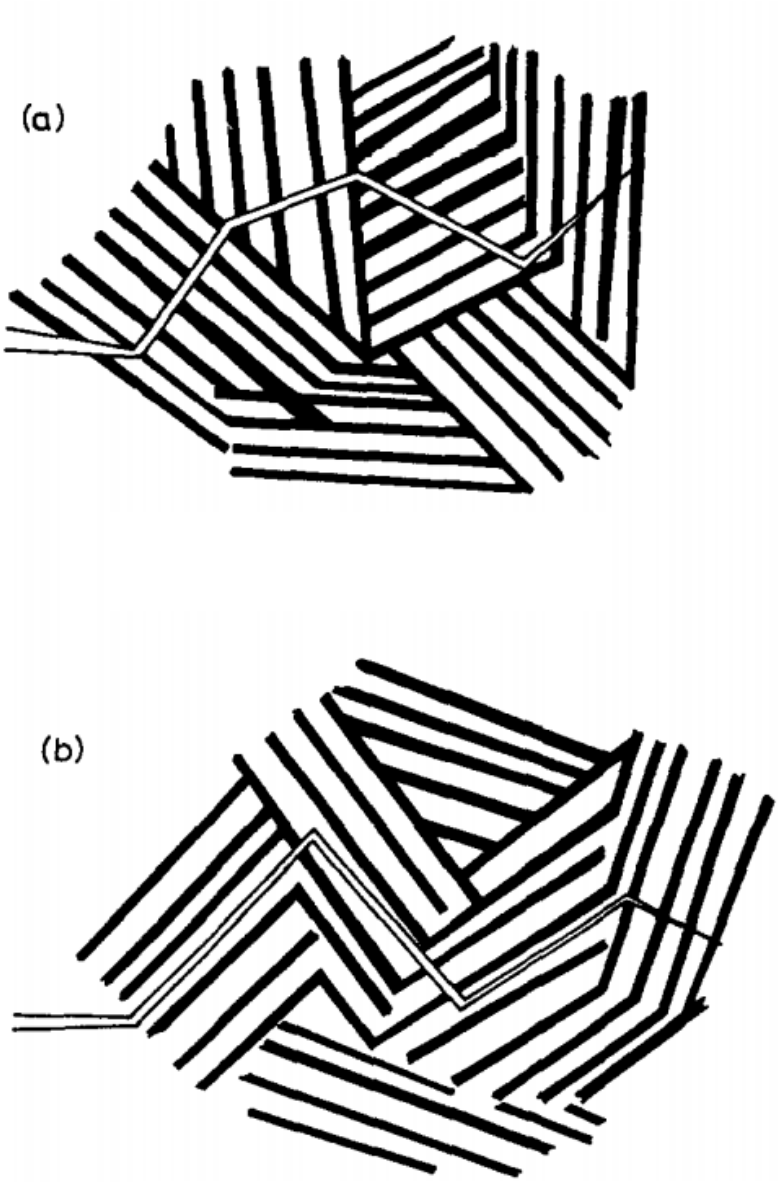

Figure 3 *- Two modes of crack growth (a) across the colony ad (b) parallel to the lamellas, both resulting in crack deflection [16].*

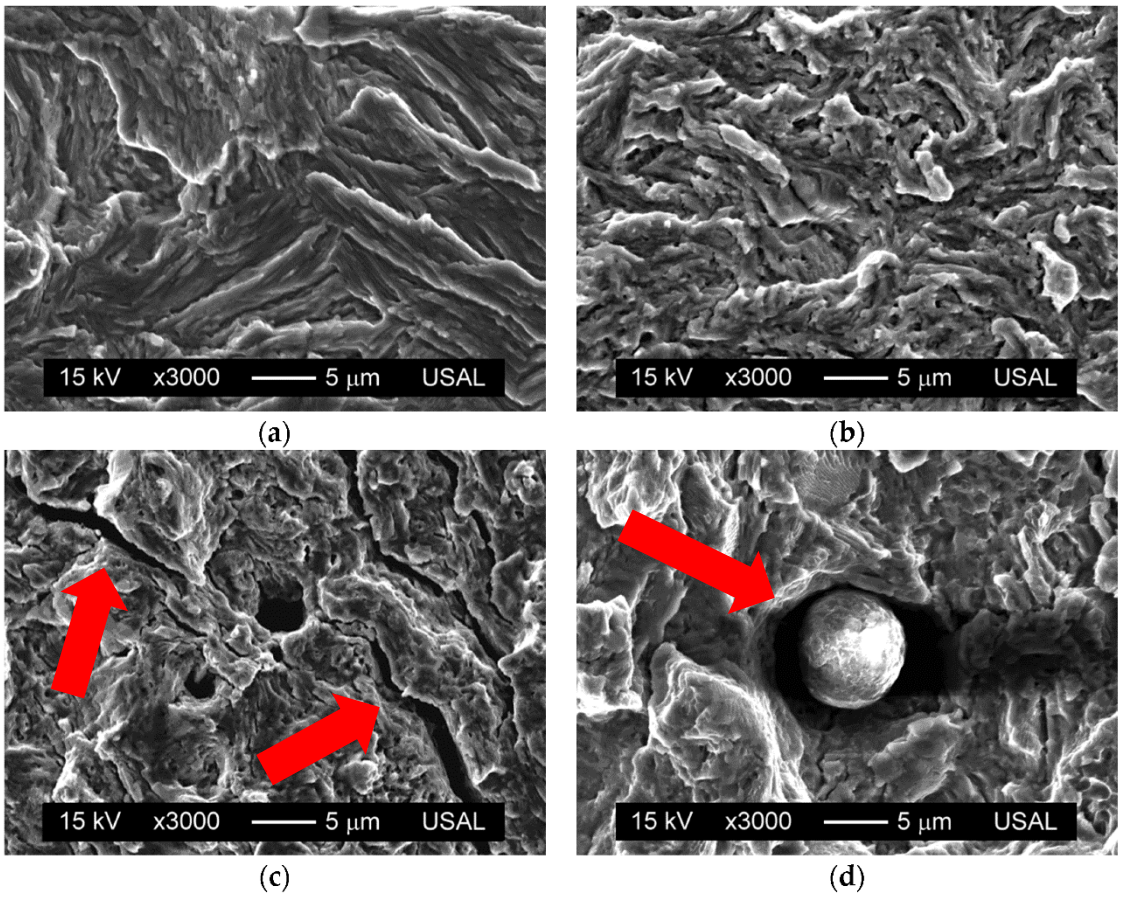

Figure 4 *- Fatigue surface fracture of a fatigue test in full pearlitic steel for (a) hot rolled bar, (b) cold-drawn wire, (c) micro-cracking and (d) a particle in the surface [19]. The images show the roughness in the fracture caused by the pearlitic microstructure.*

Toribio et al. [19, 21, 23, 24], however, observed that the fatigue cracking develops with a micro-plastic tearing, resulted by the plastic concentration in the crack tip, and ended in a brittle manner, by cleavage. They classified the fatigue crack propagation as tortuous, with micro-discontinuities, branching and local deflections, as shown in **Figures 5-a** to **5-h**. They also showed that the fracture surface roughness is more related to the deflection in the colony boundaries than in the ferrite/cementite interface [24].

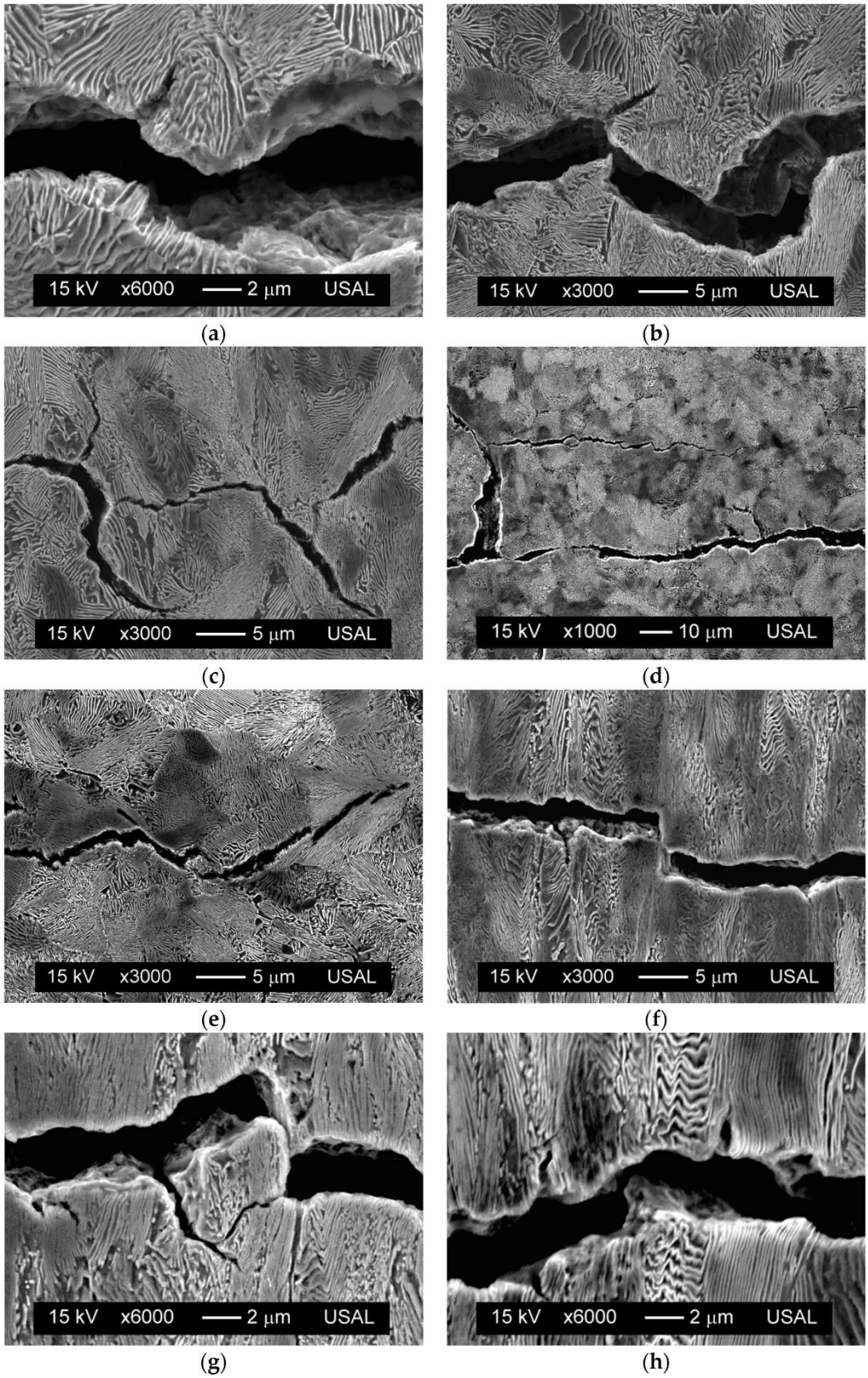

Figure 5 - *Crack paths in full pearlitic steels showing (a) micro-damage, (b) deflections caused by the pearlitic colonies, (c) branching, (d) multi-cracking, (e) micro-discontinuity, (f) interlocking, (h) debris and (h) pearlite pseudo-colony [19].*

The present study will analyze the effect of the pearlitic interlamellar spacing on the fatigue behaviour of the pearlitic steels. Two microstructures were studied: fine and coarse pearlite. The fatigue tests were programmed to control the total deformation, using values of 0.6%, 0.8%, 1.2%, and 1.6%. Additionally, the fracture surfaces, relief marks due to intrusion/extrusion couples and small cracks propagation in the surface will be characterized by scanning electron microscopy to investigate the effect of total strain and the pearlitic interlamellar spacing on the fatigue properties of pearlitic steels.

2. Materials and methods

2.1. Materials

In this study, all the specimens used in the tests of fatigue were provided by the Bekaert enterprise. The composition of the steel is described in **Table 1,** according to the standard AISI 1080. The amount of carbon in the steel is close to the eutectoid composition. This steel is destined initially for the production of wires, by the wire drawing process, described in **Figure 6**. However, for this project, the material was analyzed after the patenting phase. This stage consists of an austenitization of the material at a temperature of 950 °C for 124 seconds, followed by a fast cooling to a lead bath at isothermal temperature (540 °C or 640 °C) for 30 seconds. Finally, the material was cooled in the water at room temperature.

Table 1 *- Composition of the steel used in this study [25].*

Element	C	Mn	P	S	Si	Cu	Cr	Ni	Fe
% (wt)	0.776	0.587	0.014	0.009	0.235	0.013	0.020	0.020	Bal.

Thus, an isothermal holding in temperatures below the eutectoid temperature will generate a fully pearlitic microstructure. For this study, two different transformation temperatures were used to obtain different interlamellar distances: 540 °C and 640 °C. As expected [5, 11, 12, 13], the lower temperature generated finer pearlite (FP) with a higher hardness of 377 ± 11 HV and the higher temperature produced coarser pearlite (CP) with a lower hardness of 312 ± 9 HV. The microstructures are shown in **Figures 7-a** and **7-b**, and the values of pearlitic interlamellar distance and hardness for each material are shown in **Table 2** [25].

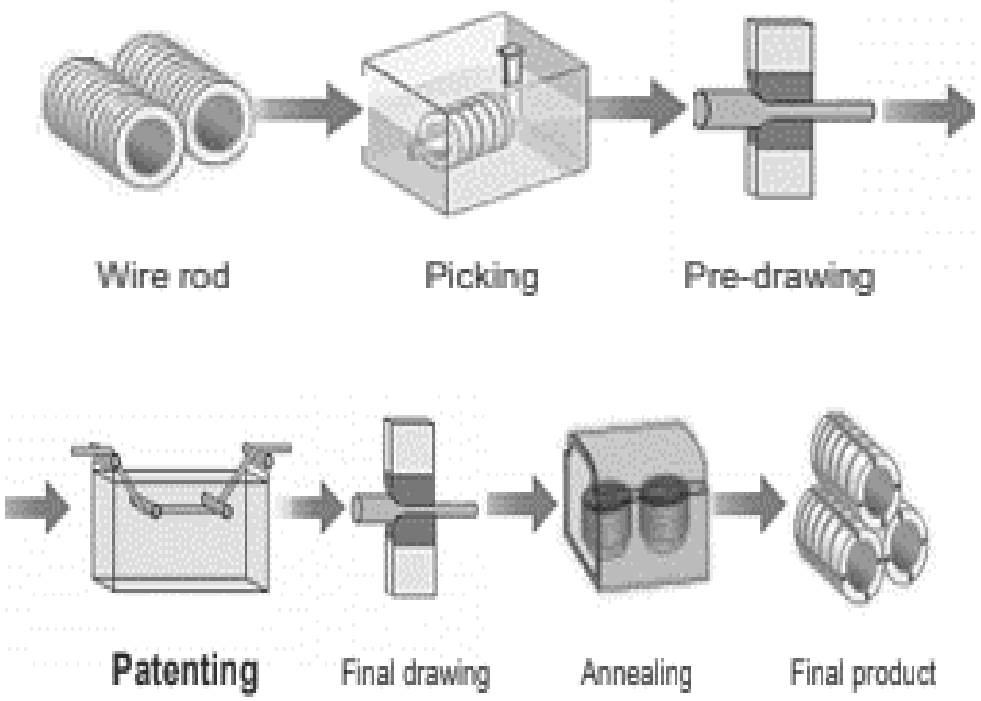

Figure 6 *- Wire drawing process [25].*

Table 2 *- Hardness and interlamellar spacing for coarse (CP) and fine (FP) pearlite [25].*

Sample	Hardness (HV)	Interlamellar space (nm)
FP	377 ± 11	72 ± 15
CP	312 ± 9	143 ± 32

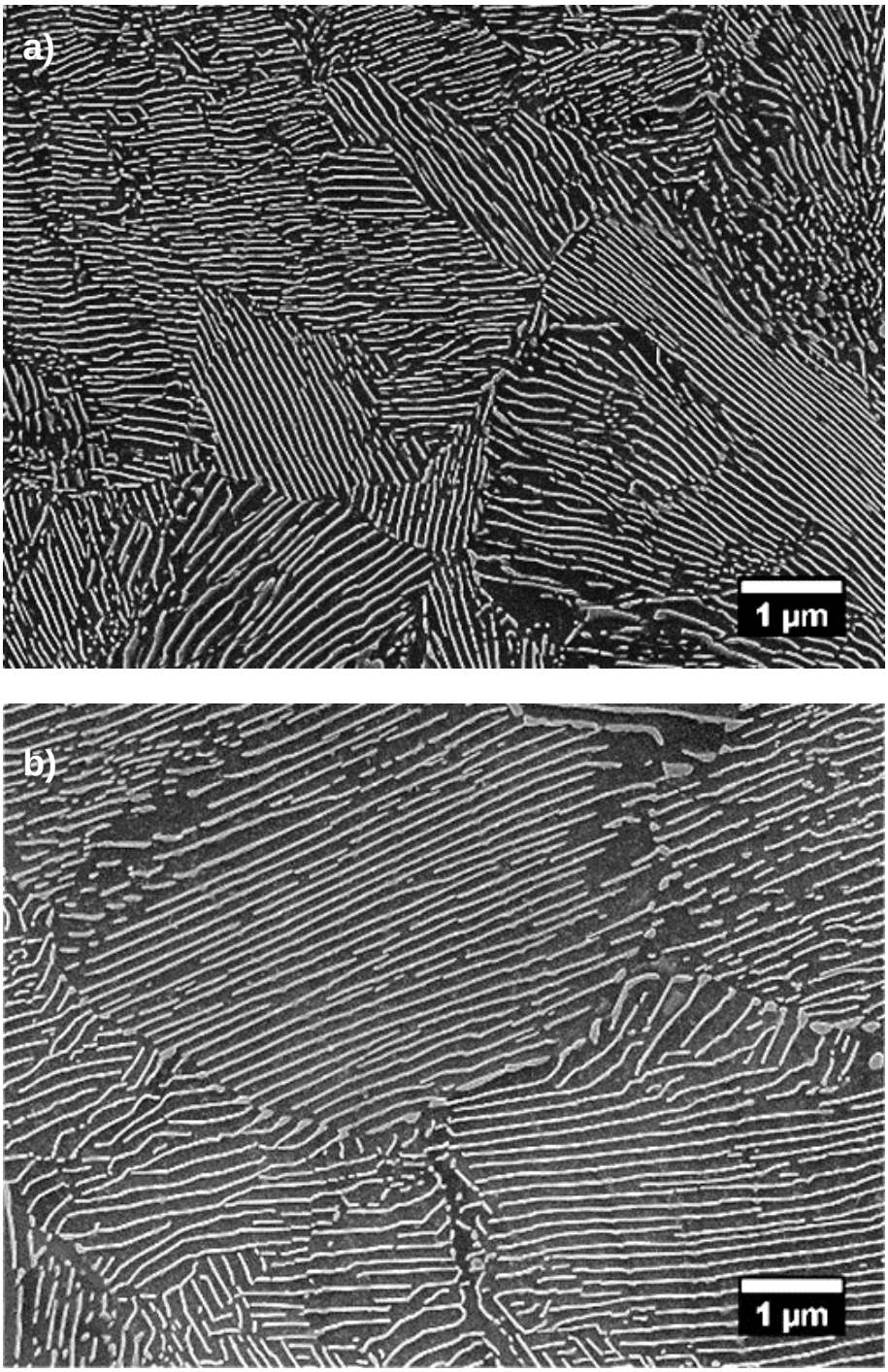

Figure 7 *– SEM-SE images of the microstructure of the wire after patenting. a) Patenting temperature is equal to 540 °C, producing fine pearlite with a lamellar space of 72 nm; and b) Patenting temperature is equal to 640 °C, producing coarse pearlite with a lamellar spacing of 143 nm [25].*

2.2. Fatigue testing

The fatigue tests were carried in an MTS 25 kN machine (see **Figure 8**), located in the laboratory Unité Matériaux et Transformations (UMET), in France. In this study, the strain-life (ε-N) approach was used [18]. So, the total deformation ($\Delta\varepsilon_t$ or $\Delta\varepsilon$) was imposed, and the force required was measured as a function of the cycle number (N). A triangular pattern was used for the deformation with a strain rate of 4.10^{-3} s^{-1}, as shown in **Figure 9**. It is important to notice that only positive values of deformation were imposed, with minimum deformation of 0.1%. Values of total deformation of 0.6%, 0.8%, 1.2% and 1.6% were used based on previous works [26]. The tests were carried until an accumulated deformation of 5% or failure. They were operated at room temperature, and the strain was measured using an extensometer and duplicates were made for all the levels of deformation.

For the tests, cylindrical specimens were used (**Figure 10**). They were carefully polished (**Figure 11**) until ¼ of micron using a diamond paste to obtain an excellent superficial finishing, essential to evaluate the fatigue properties [18]. The diameter of the screw was of 6 mm, and the diameter of the smaller section (thus the resistant one) varied depending on the polishing, but usually around 2.5 mm. Before every test, the diameter of the samples was measured to obtain a better estimation of the real stress values.

For each cycle, the stress versus strain plot can be shown, producing the hysteresis curve, as exemplified in **Figure 12**. This graphic shows the difference in the behaviour of the material between the moment the stress is increased and decreased. The difference in the strain between these two moments is the permanent deformation during cycling, the plastic deformation ($\Delta\varepsilon_p$), measured in the average stress (in this example, it is equal to zero). Thus, in full elastic behaviour, this curve would be a straight line. The elastic deformation ($\Delta\varepsilon_e$) is estimated by the difference between the total deformation ($\Delta\varepsilon$) and the plastic deformation.

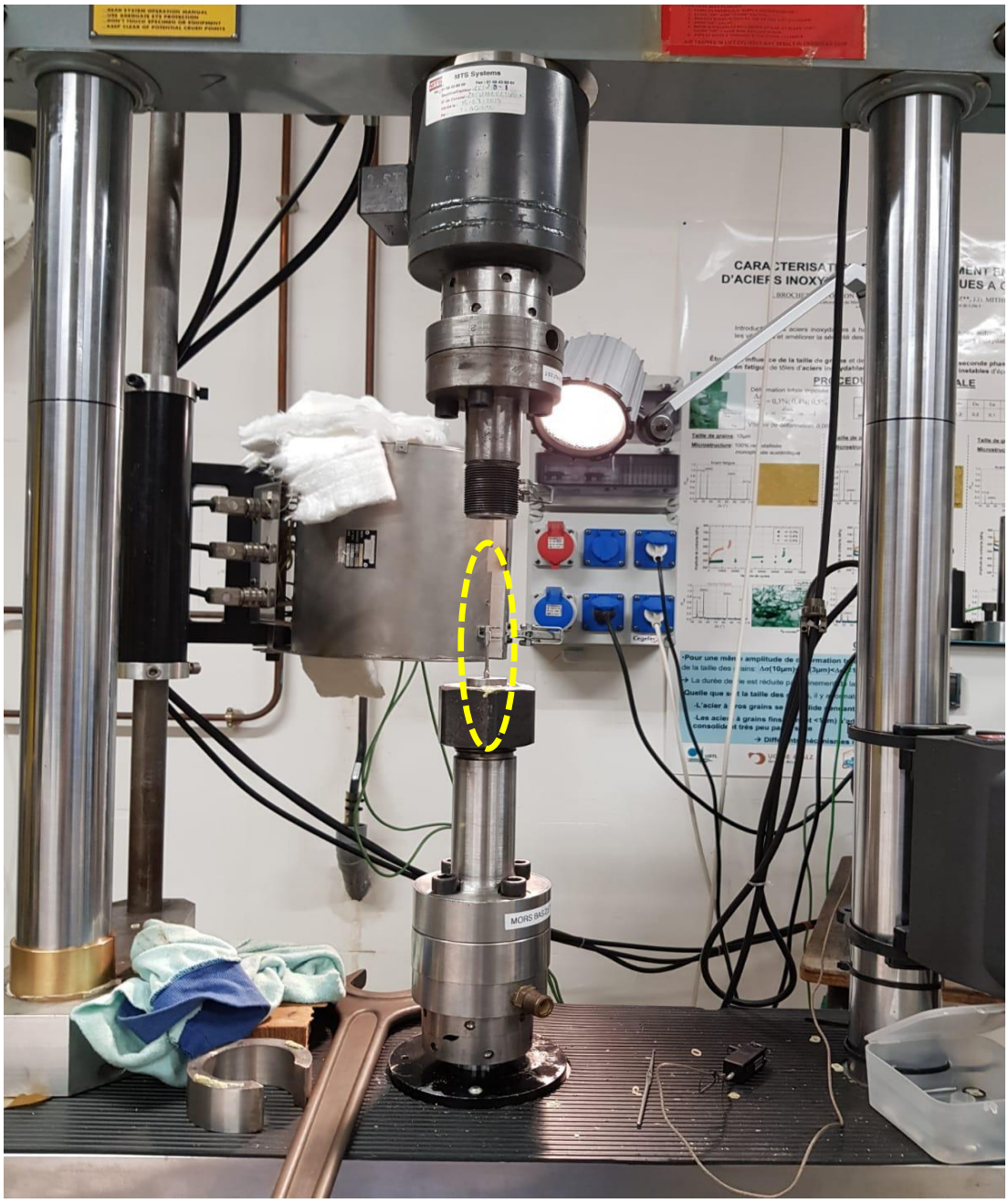

Figure 8 – *Details the MTS 25 kN machine showing in the yellow circle the position of the fatigue samples.*

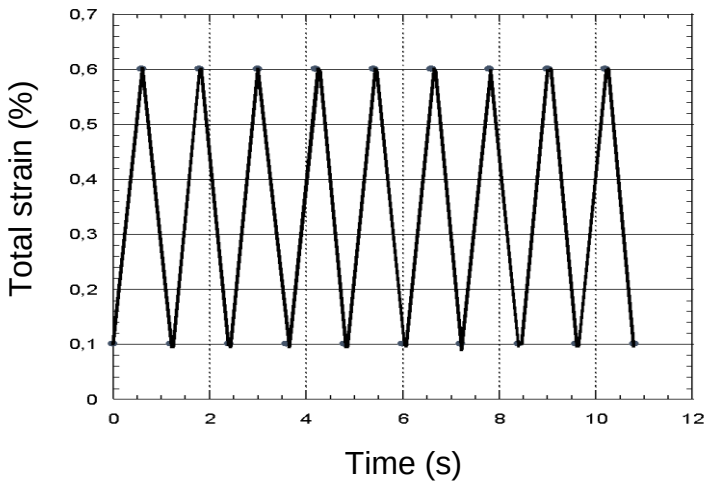

Figure 9 *- Example of the signal of the total deformation test for 0.5% total deformation, with a triangular form.*

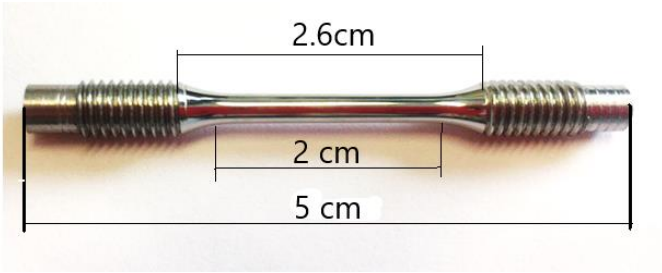

Figure 10 *- Specimen used in the fatigue test.*

Figure 11 *- The polishing process of the samples used in the fatigue tests.*

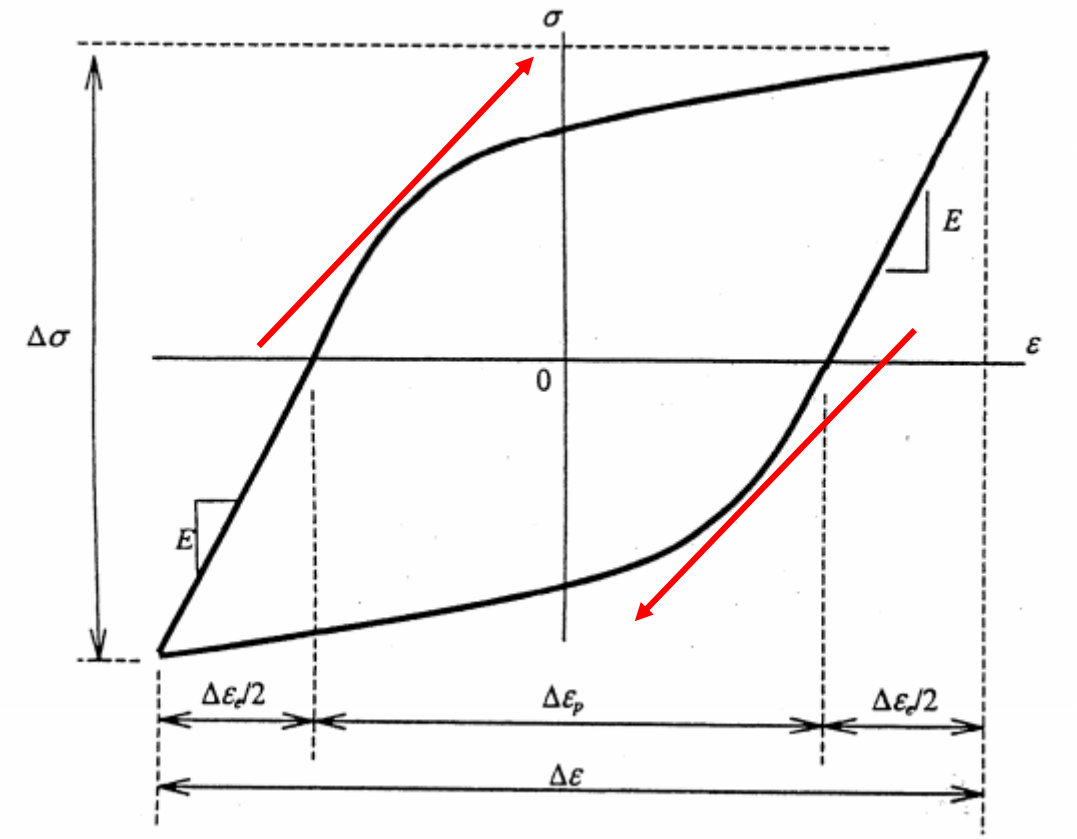

Figure 12 *- Example of a hysteresis curve, showing the plastic deformation ($\Delta\varepsilon_p$), the elastic deformation ($\Delta\varepsilon_e$) and the total deformation ($\Delta\varepsilon$), with the red arrows representing the direction of increasing or decreasing of the stress. The values of plastic and elastic deformation are measured regarding the average stress, in this case, equals to 0 [18].*

2.3. Microscopy

The scanning electron microscope images using secondary electrons (SEM-SE) were used for three main objectives: exam of the fracture surface, observation of the intrusion/extrusion marks and interpretation of the short crack propagation. For the first two proposes, an SEM HITACHI SU 5000 analytic with variable pressure was used, located in the University of Lille, with no sample preparation. For the crack propagation investigation, a HITACHI tabletop SEM, located in the UMET laboratory, was used. Only the samples subjected to a total deformation of 1.6% were cut transversally for this analysis. The surface was grinded using abrasive paper until de mash #4000, followed by a finer polishing using diamond paste until ¼ of µm and finally a more delicate surface treatment using colloidal silica (OPS) with a size of 0.04 µm followed by Picral (4% picric acid in ethanol) etching.

4. Results

4.1 Fatigue tests results

The first result that it is possible to get from the fatigue test is the cyclic accommodation graphic. The maximum and minimum values of the stress of each cycle are plotted in function of the number of cycles N. This analysis allows the observation of the how the properties of a pearlitic steel change during mechanical cycling (see **Figures 13-a** and **13-b**). To a better visualization of the data, only 0.6%, 0.8% and 1.2% total deformation data were plotted. All the results are in **Appendix A**.

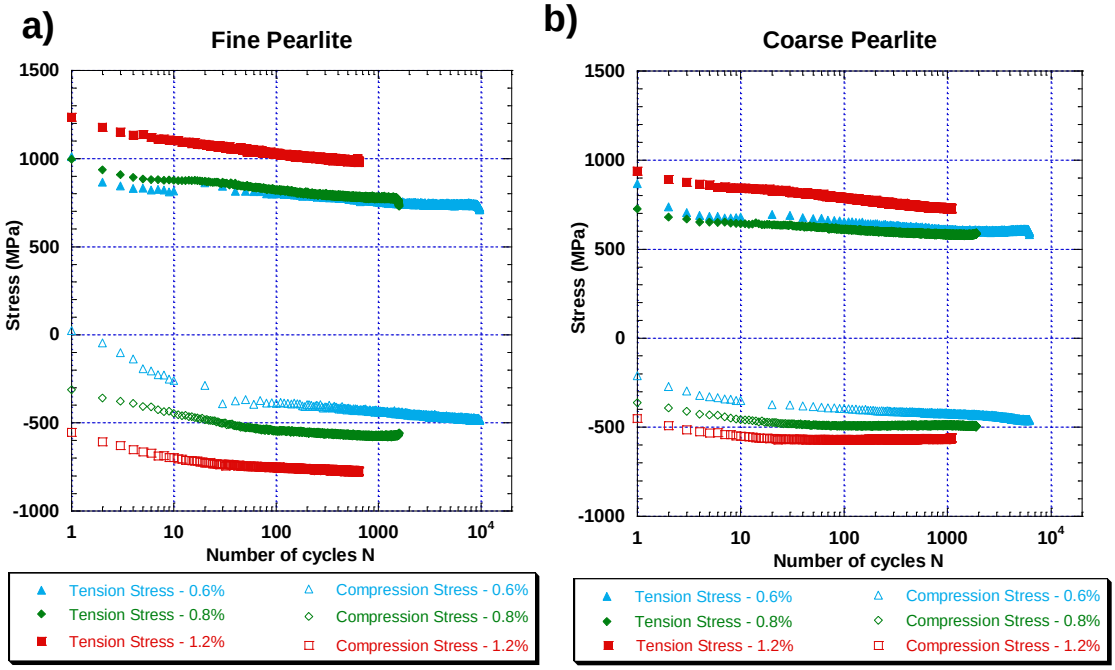

Figure 13 *- Cyclic accommodation curves of tension and compression for fine and coarse pearlite, with total deformations of 0.6%, 0.8% and 1.2%. The curve a), for fine pearlite, clearly shows the effect of softening and relaxation. In b), for coarse pearlite, the same results are noticeable, in a less drastic manner.*

The first analysis that is possible to extract in **Figures 13-a** and **b** is regarding the minimum values of stress. It is important to note that, even if the deformation is always positive, so in traction, negative values of stress are observed, characterizing a compression regime. Besides, the profiles in compression and traction are different: the differences between the values of stress in different levels of deformation are more pronounced in compression than in traction, especially for fine pearlite. For examples, analysing the curves of 0.6%

and 0.8% of total deformation, the values of stress in traction are similar, for both CP and FP. However, in compression, the values are smaller for 0.8% compared to 0.6%, especially for fine pearlite. Furthermore, when the same level of total deformation is analyzed for both samples, the required stress is different. For the fine pearlite, the stress values are always higher than for the coarse pearlite. This result agrees with the hardness obtained, 377 HV for FP and 312 HV for CP, as a harder material demands more intense stress to deform elastically. In addition, higher levels of deformation require higher stresses to be obtained for the same sample, as expected.

It is also notable a decrease of maximum tension values during cycling, meaning that there is a softening of the specimen in fatigue. For instance, when fine pearlite is analyzed with a total deformation of 1.2%, the maximum value of stress for the first cycle was around 1250 MPa, while at the end of the fatigue life it was about 950 MPa. For CP, in 1.2% of total deformation, it changed from around 950 MPa to around 750 MPa. This phenomenon becomes more remarkable as the level of deformation increases, so 1.2% shows a more drastic softening than 0.8%. In 0.8%, FP starts with a value of maximum stress of 1000 MPa and end with around 750 MPa. For CP it began at 700 MPa and ended with about 550 MPa.

It is essential to highlight that, even if the graphic shows an apparent constant softening during its fatigue life, it is in logarithmic scale. Most of the changes occur at the beginning of cycling. Its behaviour can be assumed constant during most of the test, as can be seen clearly in the graphics in the function of the fatigue life, on a linear scale, in **Appendix A**.

The hysteresis curves were plotted to understand better the behaviour of the pearlitic steels under mechanical cycling. These curves analyze what happens during one cycle, with the stress as a function of measured strain. The cycle at the middle of the fatigue life was chosen, as the fatigue behaviour can be considerate stable [18]. A high (1.2%) and a low (0.6%) level of total deformation were analyzed. See **Figures 14-a** and **14-b**.

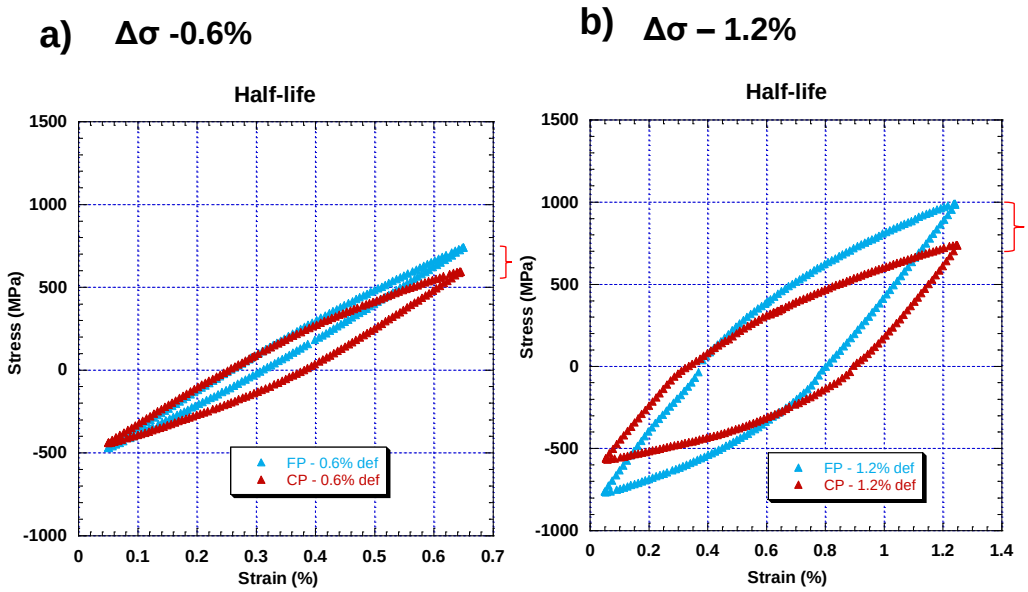

Figure 14 *- Comparison of the hysteresis loops for coarse and fine pearlite in the middle of the fatigue life. 0.6% (a) and 1.2% (b) were chosen as representatives of a low and a high level of total deformation, respectively. The maximum stress to deform FP increases more from 0.6% to 1.2% in comparison to the coarse pearlite, shown by Δσ. CP shows a higher plastic deformation than FP.*

Figures 14-a and **14-b** show that the increase of maximum stress with the increase of total strain is not the same for coarse and fine pearlite. Fine pearlite requires a higher increase in stress to deform, show by the increase in Δσ from 0.6% to 1.2% of total deformation. This indicates that fine pearlite is more resistant to deformation, so it presents a higher Young's module. Furthermore, the plastic deformation, as defined in **Figure 12**, is more prominent for coarse pearlite. All hysteresis curves for half-life are shown in **Appendix A**.

A global vision of the behaviour in fatigue of both pearlitic steels can be obtained by plotting the results of plastic, total and elastic strains for a stable situation (in this project was adopted the half life cycle) as a function of the number of cycles until failure for all the levels of total deformation. Those values were determined as described in **Figure 12**. This curved is called strain life curve. The results are shown in **Figures 15-a** and **15-b**.

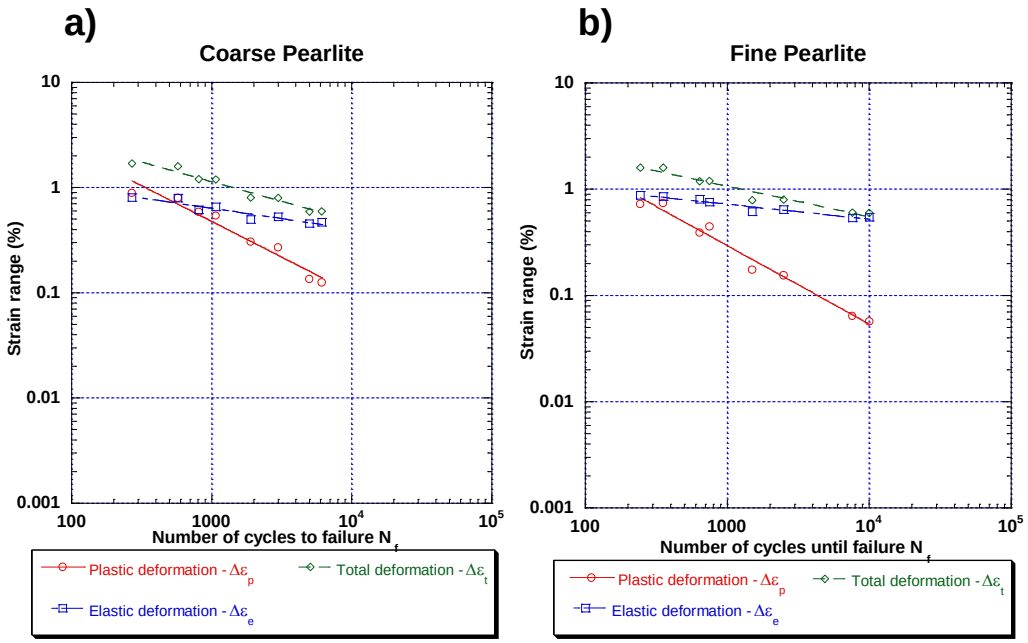

Figure 15 *– Graphics for coarse (a) and fine (b) pearlite showing the total (green), elastic (blue) and plastic (red) strains as a function of the number of cycles until failure.*

Figures 15-a and **15-b** show that for lower values of fatigue life, the deformation percentage of plastic deformation is higher, while for longer lives, elastic deformation is predominant. Both plastic and elastic deformations reduce as the fatigue life increases. However, plastic deformation changes significantly more than elastic deformation, for both samples. Thus, there is a certain level of total deformation in which the general behaviour changes from most elastic to most plastic. For the coarse pearlite, this point is well defined when total deformation values around 1.4%. In fine pearlite, this value is not determined using the data obtained in the tests, but it can be stipulated that this turning point would be fount when total deformation values around 2%.

4.2. Fracture surface

4.2.1. Fine pearlite

After the rupture in the fatigue test, the fracture surfaces of the specimens were analysed using SEM-SE. For fine pearlite at 1.6%, 1.2% and 0.8% of total deformation, specimens presented two distinct zones, with a defined interface between them, as in **Figure 16**. The first zone, marked as 1, has an elliptical shape with the centre in the region indicated by the red circle. Both zones are plane, with zone 1 being brilliant.

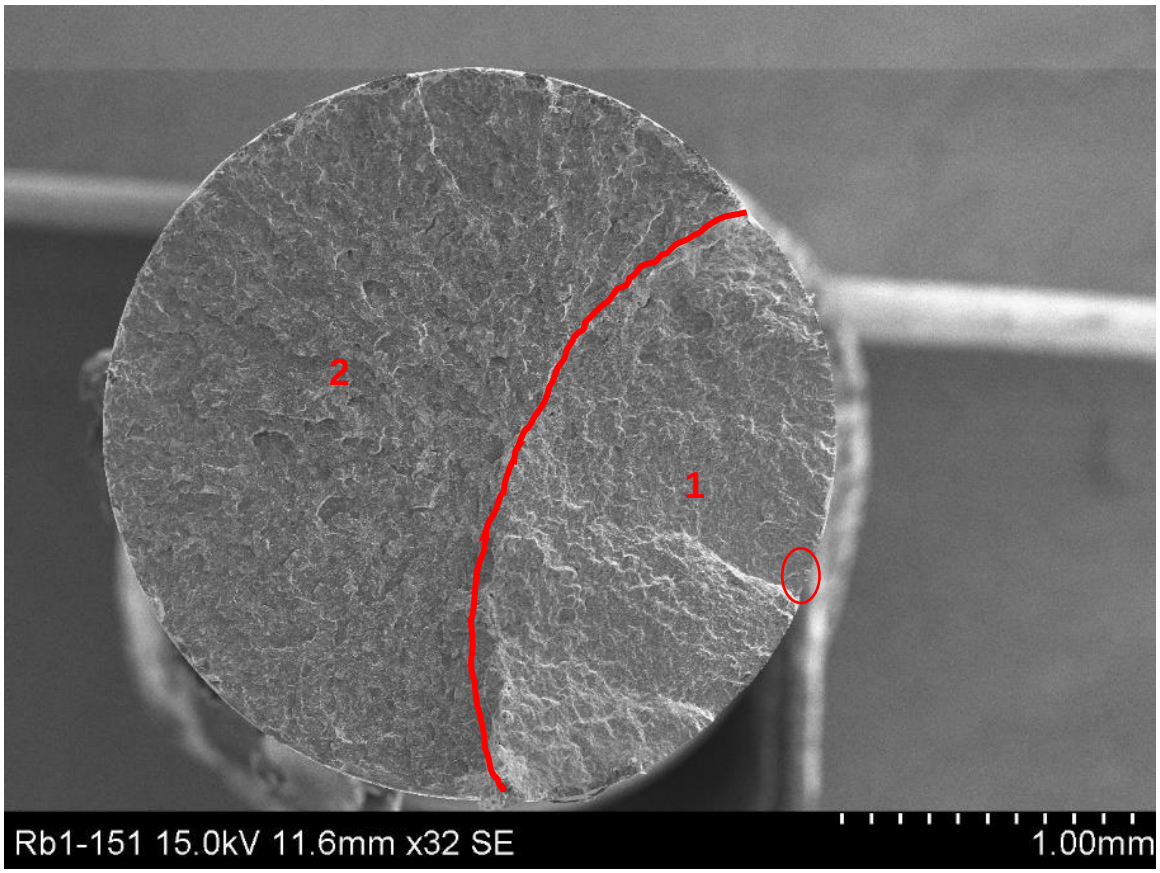

Figure 16 *- Fracture surface for fine pearlite 1.2% of deformation, with microplastic tearing in zone 1, unstable crack propagation with a river patter in zone 2 and a well-defined interface with the presence of dimples.*

A close observation of zone 1 is shown in **Figure 17**. In it, we can see the presence of microplastic tearing, highlighted by red arrows. This is a result of localized plastic deformation in the pearlitic structure. Thus, those marks have the same orientation as the pearlitic microstructure in which it is located. It is also

possible to observe some secondary cracks, which propagate in a tortuous manner, highlighted by yellow circles.

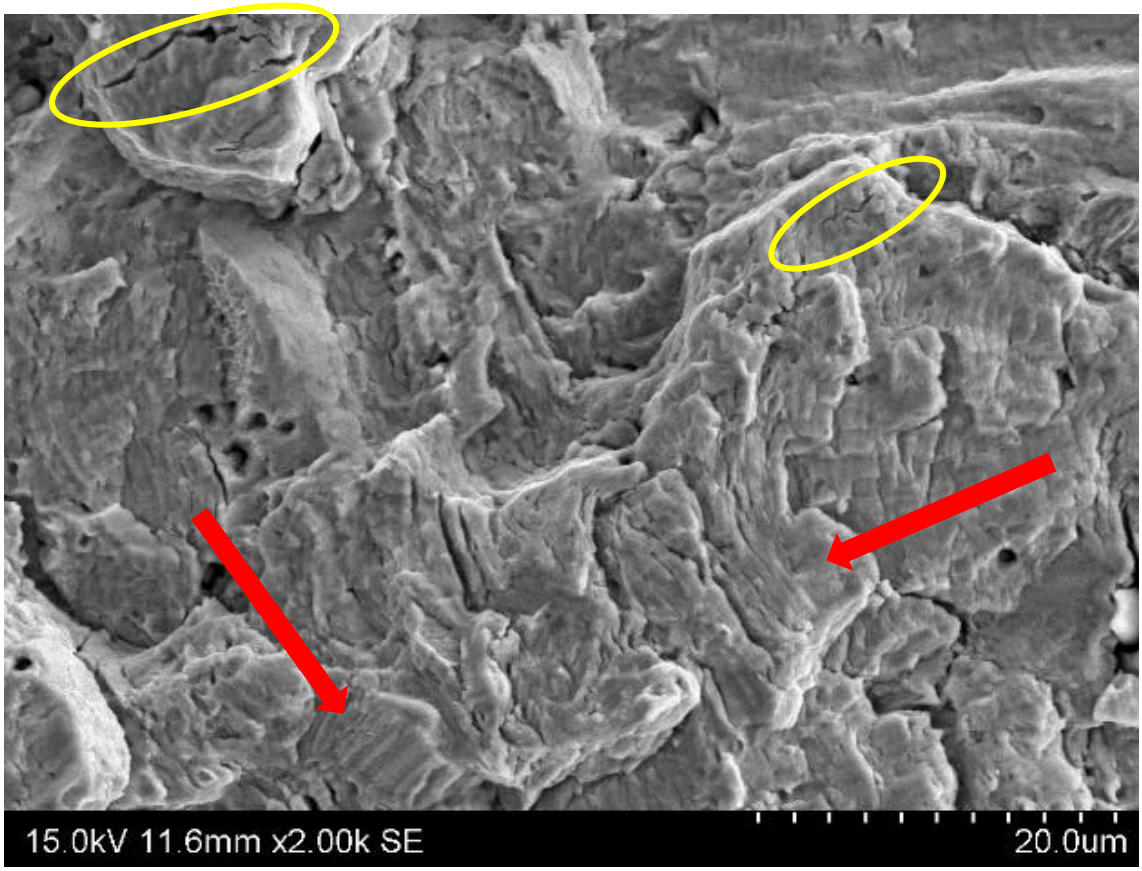

Figure 17 *- Starting fatigue zone (in this case, for FP and 0.6% of total deformation). The red arrows show the microplastic tearing of the pearlite, while the yellow circles highlight the cracks in the fracture surface.*

In the interface between zones 1 and 2, shown in **Figure 18**, it is possible to observe the presence of dimples, characteristics of plastic deformation. Those dimples are just observed in a small area in a well-defined transition zone. This was observed for all the total deformation levels of 1.6%, 1.2% and 0.8%.

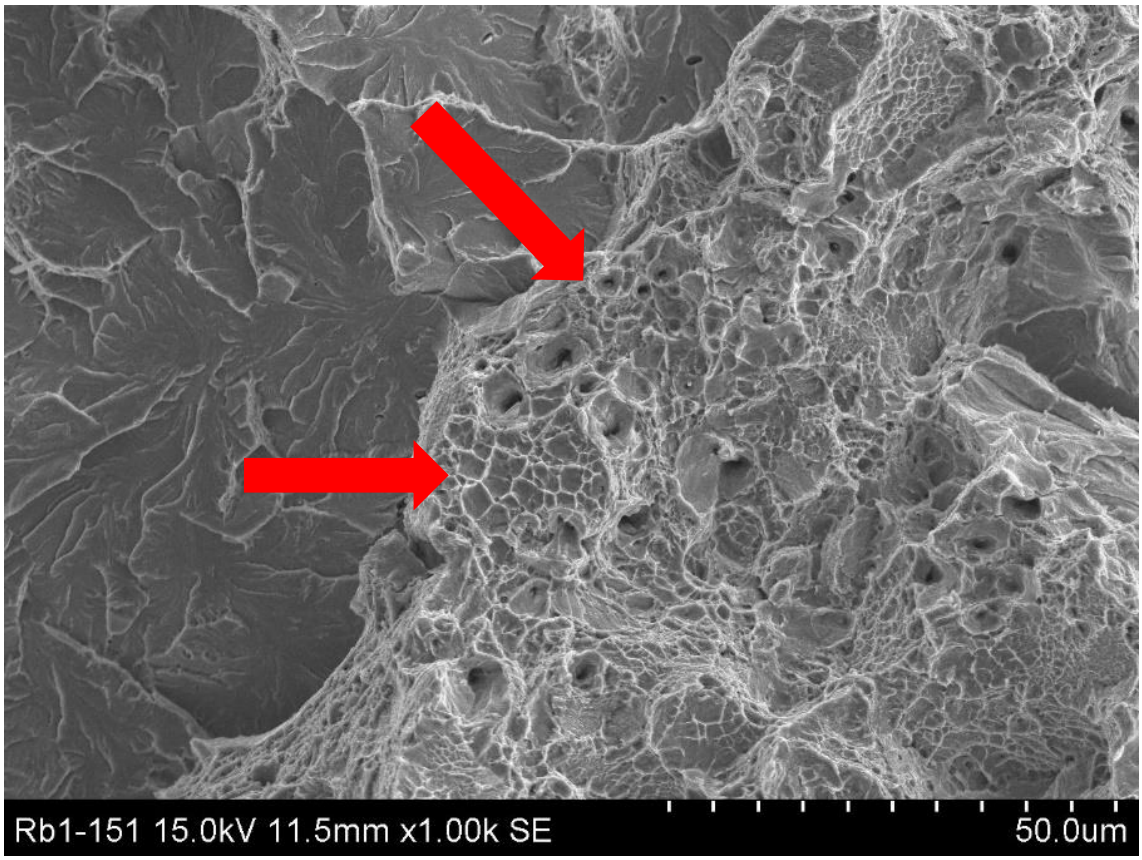

Figure 18 - *Ductile transition zone (in this case, for FP and 1.2% of total deformation). The red arrows show the dimples due to deformation.*

Finally, in zone 2 (**Figure 19**), it is possible to observe the presence of a river pattern, indicates by red arrows. This is consistent with an unstable crack propagation, with an appearance similar to cleavage. Therefore, it is possible to affirm that the fatigue crack started in zone 1, with a stable propagation, and finished with a brittle unstable propagation, with a well-defined ductile transition zone.

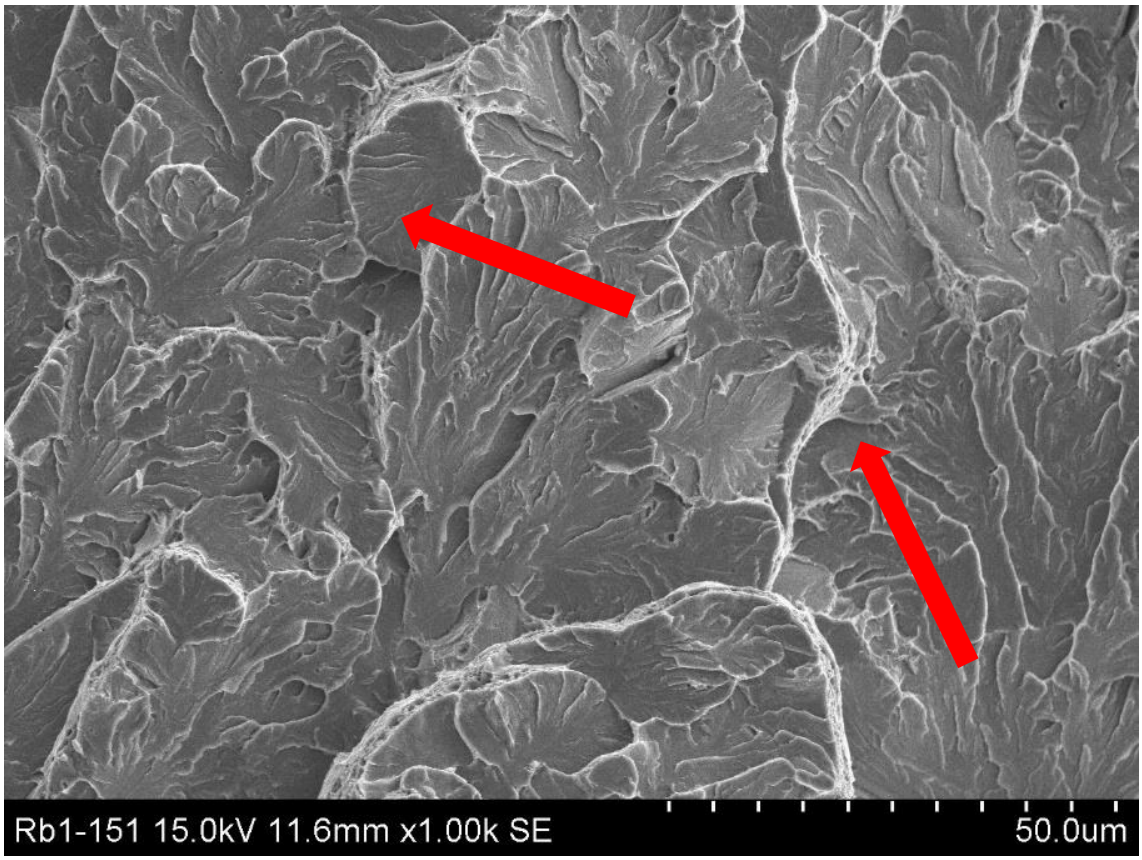

Figure 19 *- Example of the brittle final crack (in this case, for FP and 1.2% of total deformation).*

The fracture showed above is representative of the behaviour observed for fine pearlite with 0.8%, 1.2% and 1.6% of total deformation. However, the level of 0.6% showed a different profile, as observed in **Figure 20**.

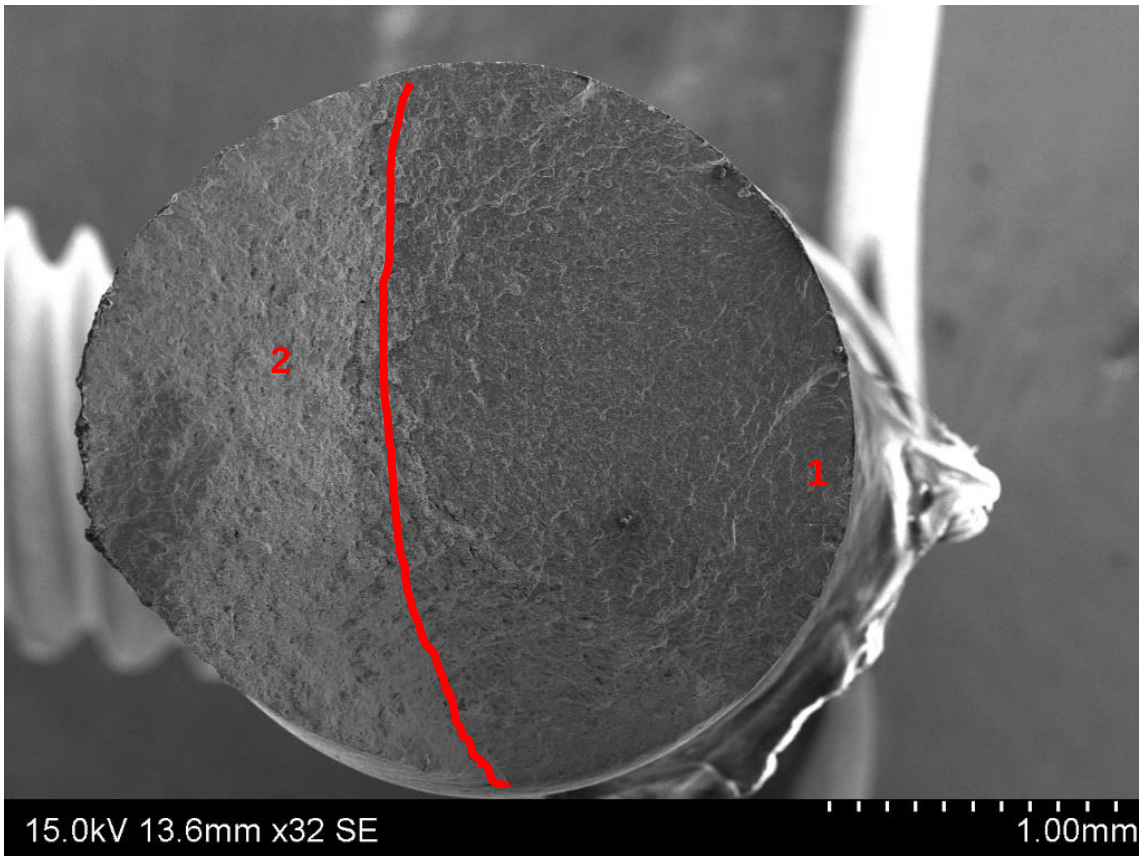

Figure 20 *- Fracture surface for FP 0.6% of total deformation, where zone 1 is the first crack propagation by microplastic tearing and zone 2 a ductile fracture, forming a high angle with zone 1 and presenting dimples*

In **Figure 20**, the zone 1 presented the same structure as in **Figure 17**, with the presence of microplastic tearing. However, the final fracture zone, unlike for the other levels of deformation, was not plane. It formed a strong angle with zone 1. Closer observation of zone 2 (**Figure 21**) showed the presence of dimples, indicating a final fracture with strong plastic deformation. There was no transition zone as in the other cases.

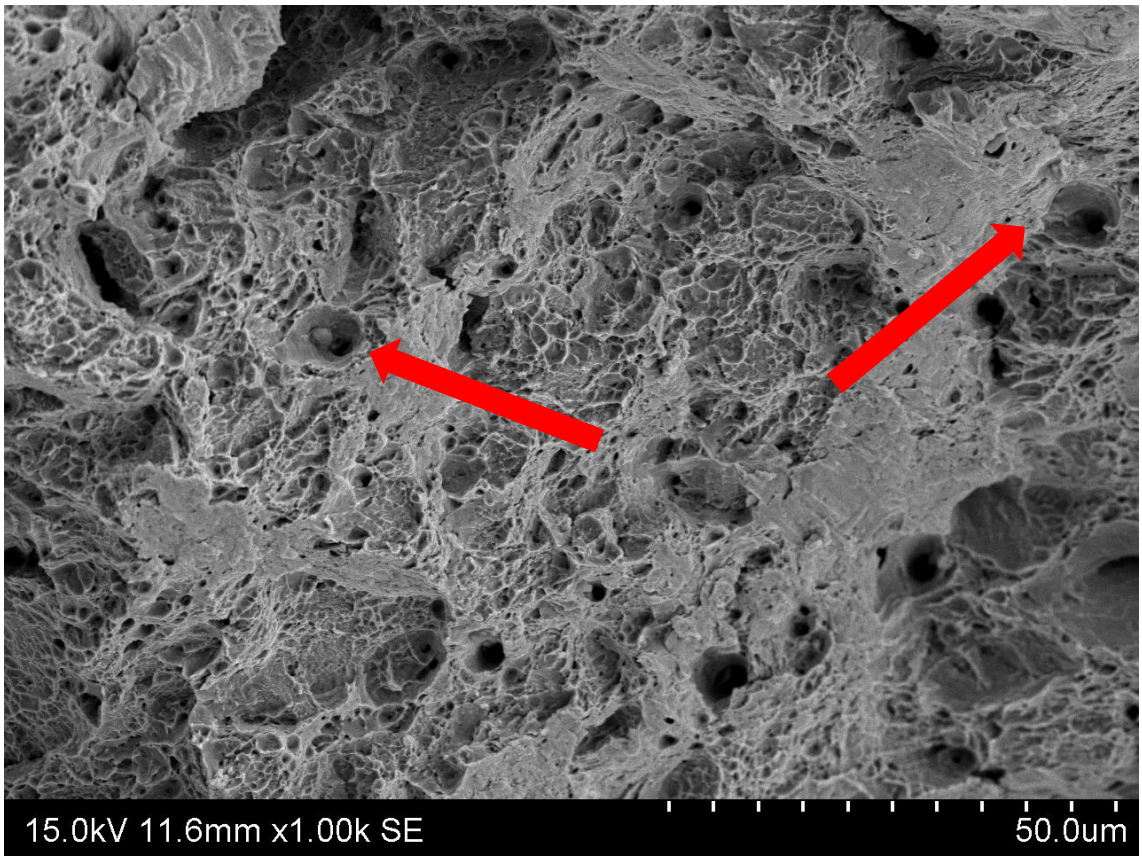

Figure 21 *- Ductile fracture for FP 0.6% of total deformation in zone 2, showing the presence of dimples, highlighted by the red arrows.*

4.2.2. Coarse pearlite

The fracture surfaces of coarse pearlite at 1.6% and 1.2% of total deformation were similar to what was observed for fine pearlite in higher levels of deformation, as it shows in **Figure 22**. Two zones well defined and plane are observed, with the first having an elliptical shape.

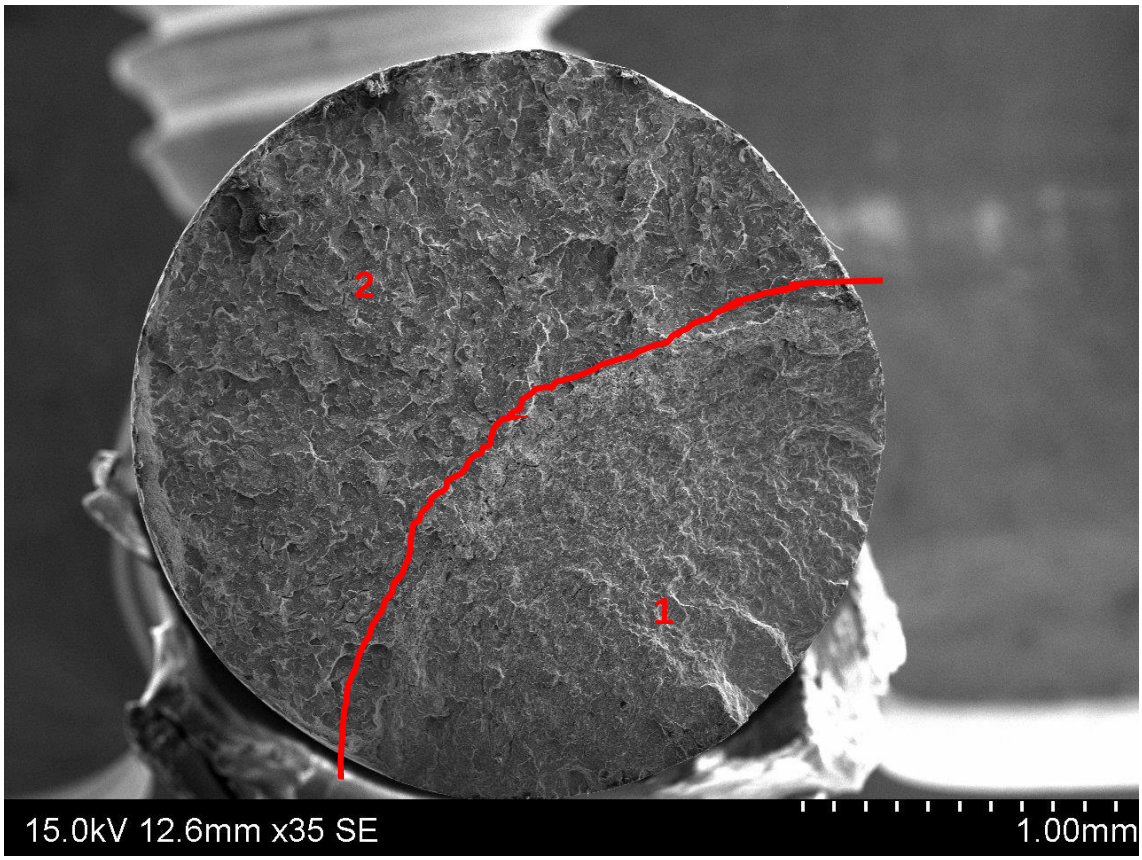

Figure 22 - *Fracture surface of the CP sample at 1.2% of total deformation, with zone 1 presenting microplastic tearing, zone 2 rivers marks in a cleavage-like fracture and an interface with dimples.*

A closer observation of zone 1 showed the presence of microplastic tearing, indicating the incitation zone, as it can be seen in **Figure 23**. Zone 2 showed the presence of rivers marks, indicating unstable final propagation by cleavage (as in **Figure 24**) and the interface showed the presence of dimples (**Figure 25**).

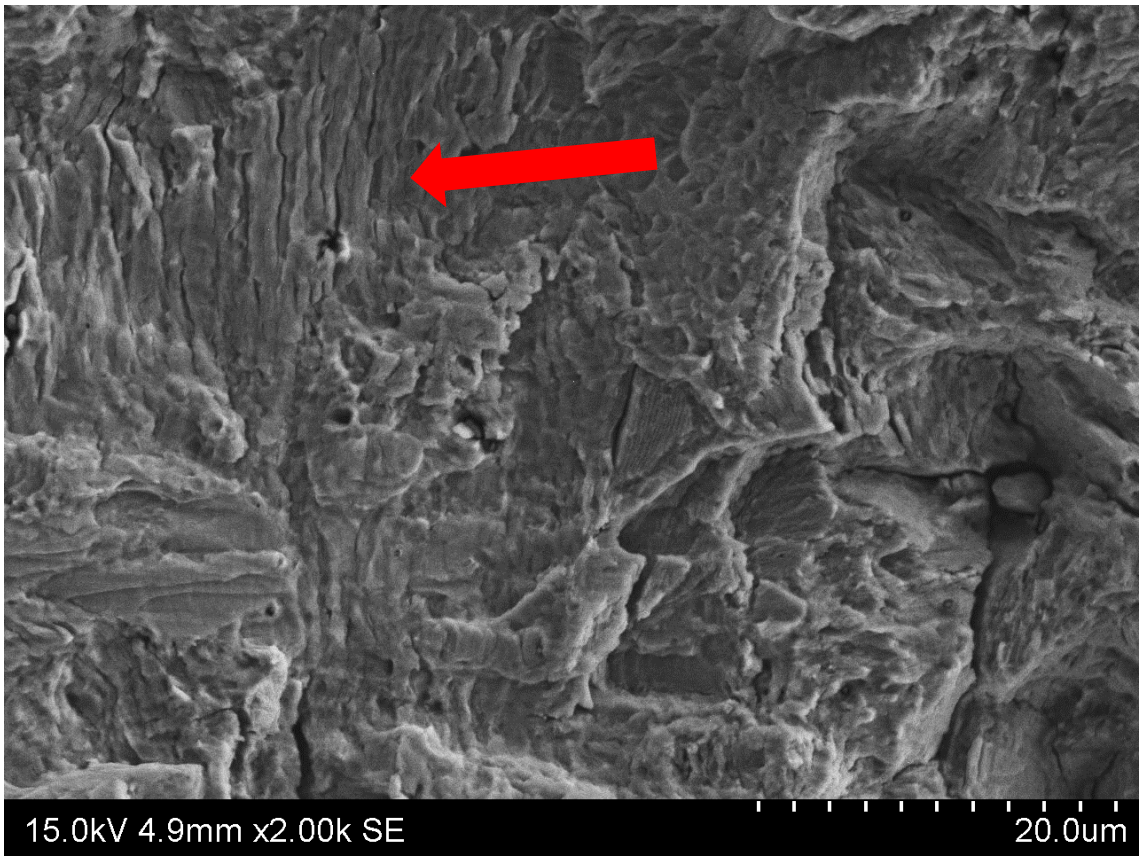

Figure 23 *- Fracture surface of CP at 1.2% of total deformation in zone 1. This image shows the presence of microplastic tearing, highlighted by the red arrow, indicating the stable propagation of the crack in fatigue.*

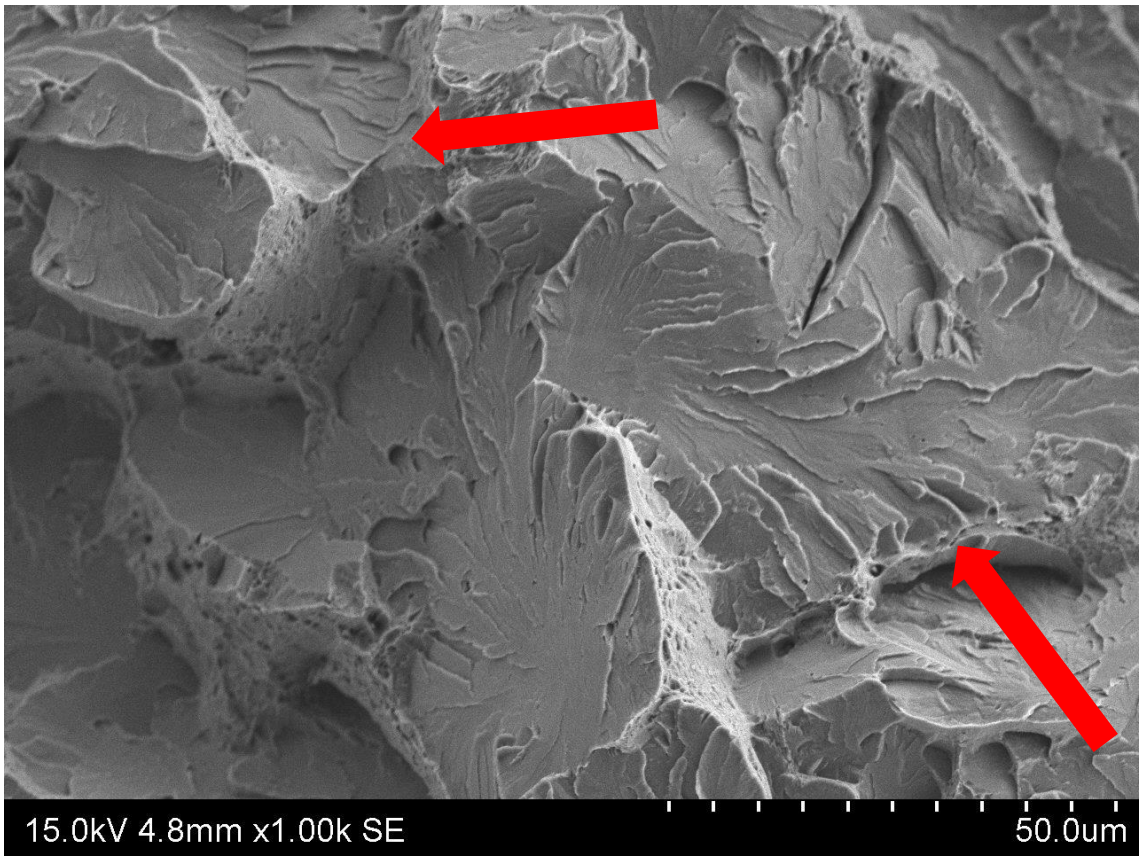

Figure 24 *- Fracture surface of zone 2 in CP at 1.2% of total deformation. It is possible to see the presence of rivers marks, indicated by the red arrows, suggesting an unstable propagation by cleavage.*

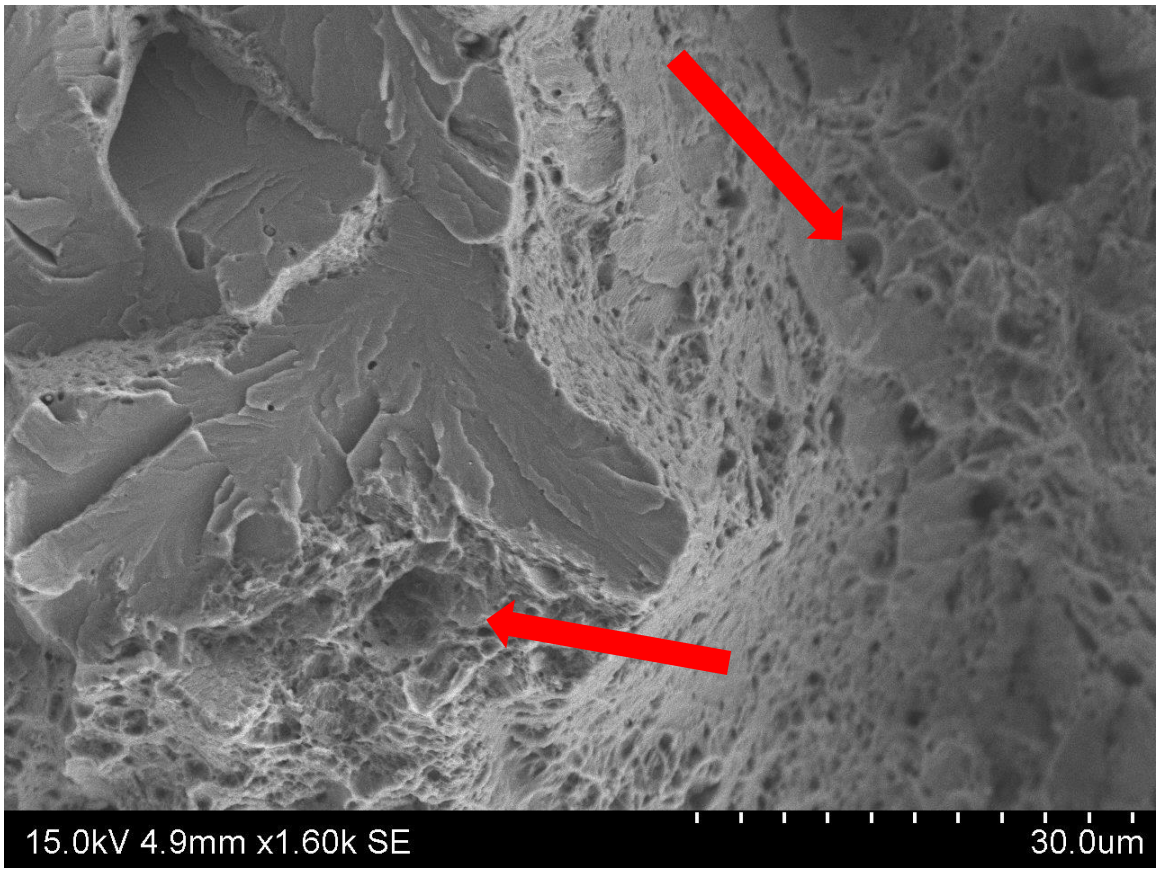

Figure 25 *- Fracture surface of the interface between zones 1 and 2 for CP at 1.2% of total deformation. It is possible to observe the presence of dimples, indicating plastic deformation, highlighted by the red arrows.*

For lower levels of deformation (0.8% and 0.6%), however, the behaviour changes, as it was observed for fine pearlite, as observed in **Figure 26**. Zone 1, plane, showed the presence of microplastic tearing, as in **Figure 23**. The zone 2, of final fracture, formed a high angle with zone 1. In addition, further observation of zone 2 (see **Figure 27**) showed the presence of dimples, indicating ductile fracture. A transition zone was observed, as highlighted in a red circle in **Figure 26**. Closer observation of this zone showed the presence of rivers marks, as in **Figure 24**. The presence of this transition zone is the main difference when coarse pearlite at 0.8% and 0.6% of total deformation is compared to fine pearlite at 0.6%. All the fracture surfaces for both coarse and fine pearlite are shown in **Appendix 2**.

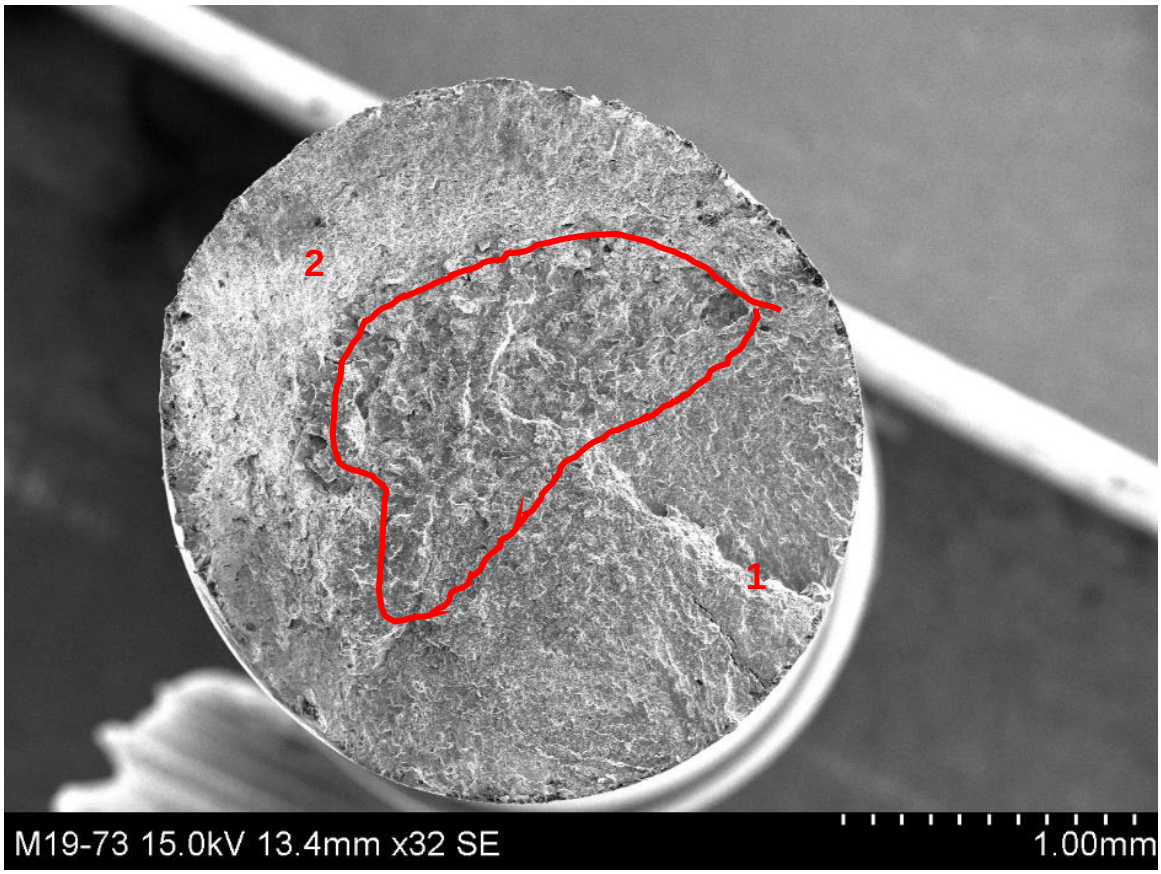

Figure 26 *- Fracture surface of coarse pearlite 0.6% of total deformation, with a microplastic tearing in zone 1, a brittle transition zone highlighted with a red circle and a final ductile fracture in zone 2, forming a high angle with the rest of the fracture surface and presenting dimples.*

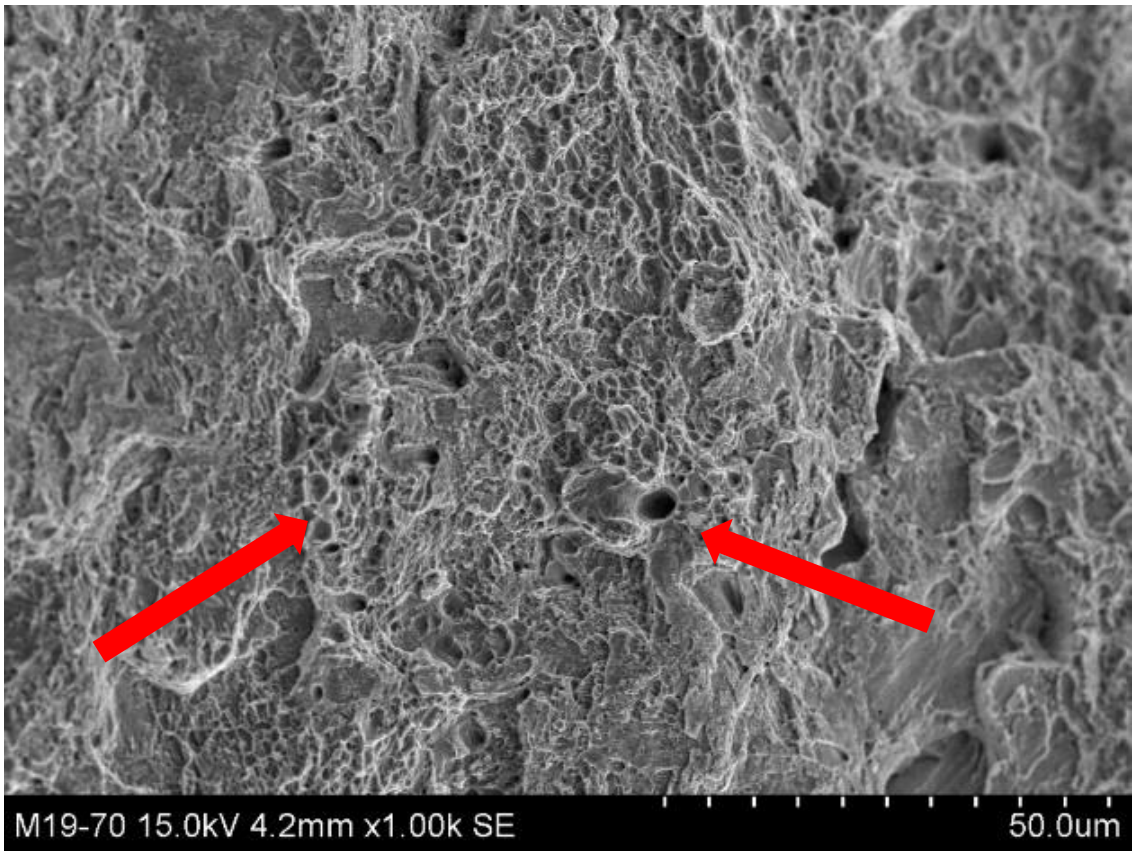

Figure 27 - *Ductile final fracture for coarse pearlite at 0.8% of total deformation in the zone 2, the final fracture zone. The dimples formed due to plastic deformation are highlighted by red arrows.*

4.3. Surface topography marks

The analysis in the scanning electron microscope (SEM) of the surface of the specimen allows the observation of the topography. As it was observed by **Figures 14** and **15**, there is plastic deformation during fatigue. Those plastic deformations will create intrusions and extrusions along with the slip plans of the material. **Figures 28-a** to **28-d** show the images for coarse and fine pearlite at 1.2% and 1.6% levels of total deformation, where the red arrows represent the load direction. In **Figures 28-a** to **28-d**, it is remarkable that, for the coarse pearlite, the surface topographic marks (intrusions, extrusions and cracks) are more prominent and more present. Even though those marks are more evident in high levels of deformation, they were observed in lower levels of deformation for coarse pearlite, but not in fine pearlite, probably due to the small size of those marks in those cases.

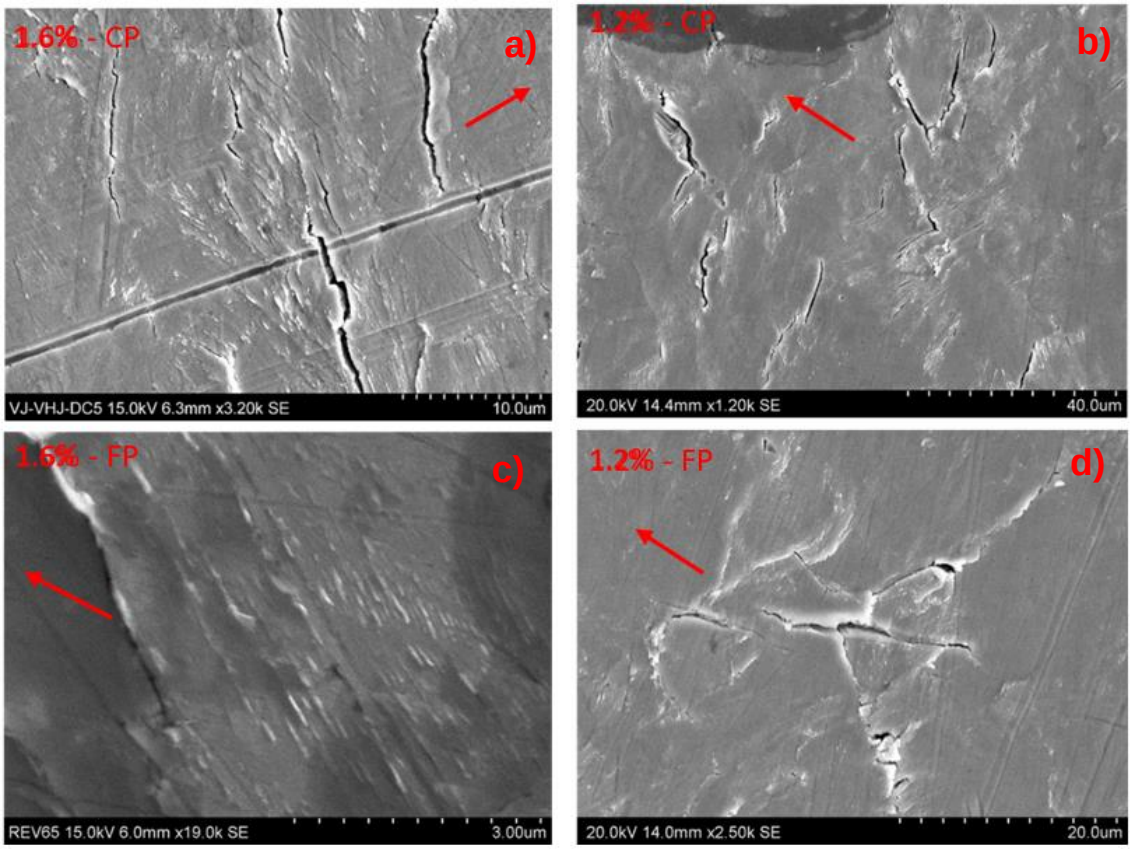

Figure 28 – *Intrusion and extrusion marks and cracks for coarse pearlite at 1.6% (a) and 1.2% (b) and fine pearlite at 1.6% (c) and 1.2% (d) of total deformation. The image shows that*

coarse pearlite presents numerous and larger marks than the finer. The marks and cracks were more prominently present in 1.6% of total deformation. The red arrow represents the load axis direction.

4.4. Small crack propagation

The small cracks are the cracks that nucleated at the surface, in the intrusion/extrusion couples, but did not grow big enough to cause the failure. A transversal cross-section of the sample was made to analyze the small crack propagation. It was chosen to only study this behaviour for CP and FP for 1.6% of total deformation, as they are the samples with the highest amount of intrusion/extrusion couples, hence the more likely to have well-developed cracks. The images obtained are shown in **Figures 29-a** and **29-b**. The figures show that the mechanism of crack propagation is similar for both interlamellar spacings. For both cases, the propagation of the crack is transgranular, In the coarse pearlite samples, the crack seems to firstly propagate in a straight direction and deflected when encountering another colony of pearlite.

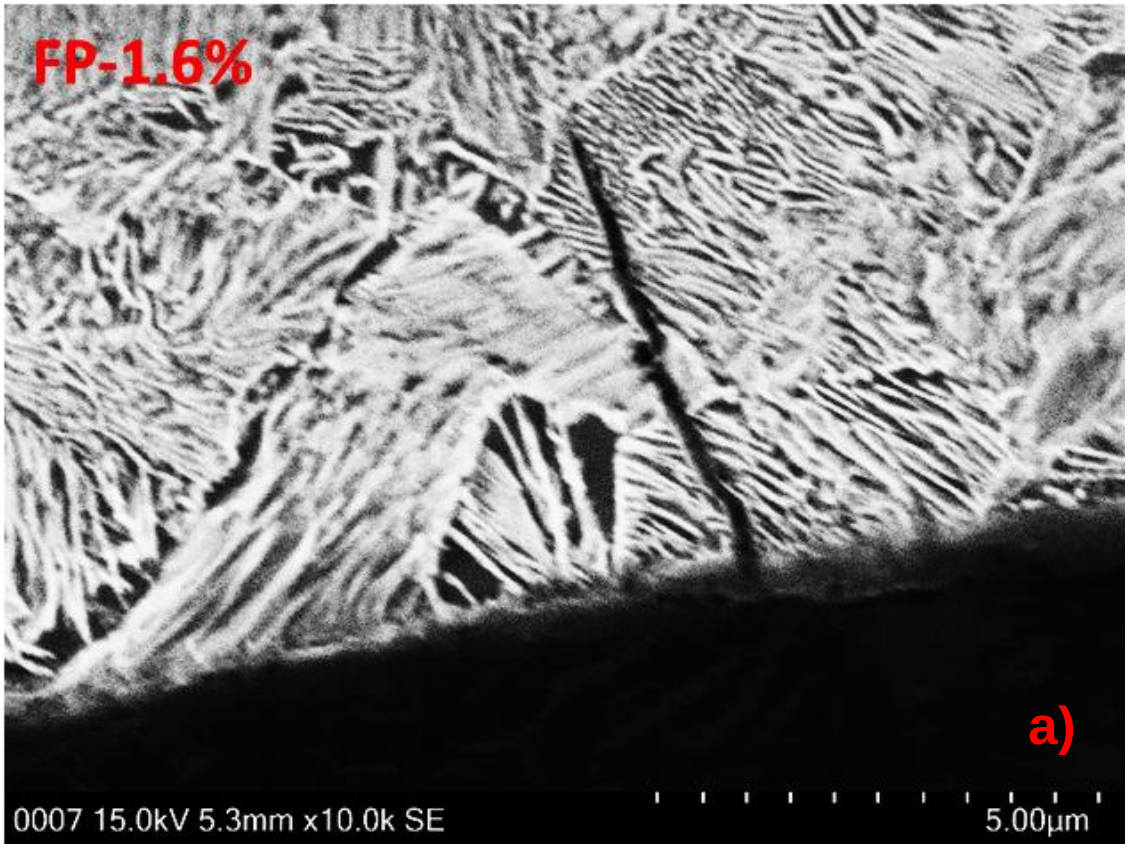

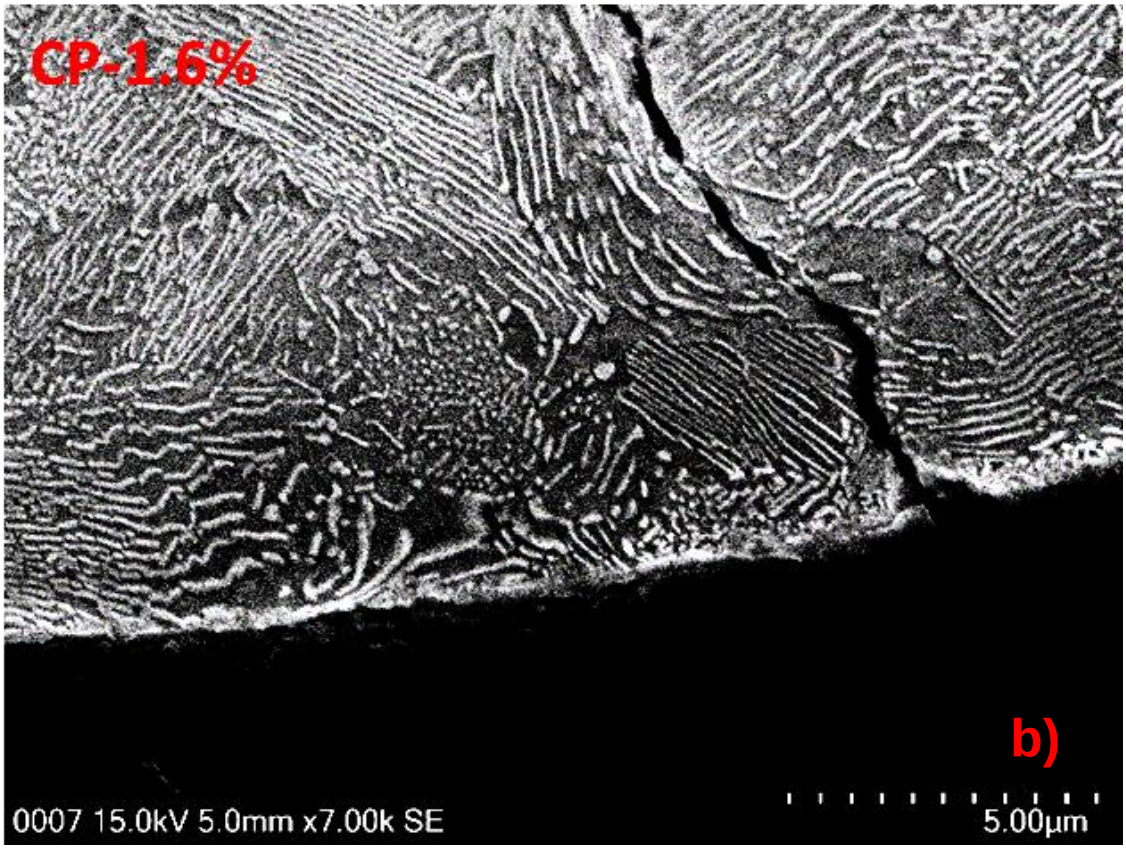

Figure 29 *– Longitudinal section of small crack propagation for 1.6% of total deformation. The samples were etched with Picral. In (a) fine pearlite and (b) coarse pearlite the crack nucleates in a transgranular path. In coarse pearlite, it is possible to see a deflection of the crack propagation when another colony of pearlite is encountered.*

5. Discussion

When fatigue tests were operated, both coarse and fine pearlite showed relaxation behaviour, probably since pearlite is a strong microstructure, accumulating a high density of dislocations in the interface ferrite/cementite [3]. Thus, during cycling, the dislocations network reorganizes, reducing its density. Also, the reduction in both minimum and maximum values of stress is characteristic of fatigue tests using the ε-N model when the relation between the minimal and maximum value of strain is different from -1. This relaxation is a result of plastic deformation during cycling. Hence, the higher the stress amplitude, the higher the relaxation effect, as it was observed in **Figure 13**. Finer pearlite is harder and thus required higher stress to obtain the same strain amplitude. Also, finer pearlite is less susceptible to deformation, requiring higher stress amplitudes to move to higher levels of strain amplitude in comparison to coarse pearlite, as shown in **Figure 14**. This is expected [5, 11, 12, 13] due to the Hall-Petch effect of the interlamellar spacing, so FP is a harder material (377 HV compared to 312 HV for CP) with a higher Young's modules. This also results in the amount of plastic deformation observed in the hysteresis curves (**Figure 14**). Softer coarse pearlite deformed more plastically during cycling than fine pearlite.

The analysis of **Figures 15-a** and **15-b** confirms that finer pearlite is harder to deform plastically, as the point where the plastic deformation becomes more important than elastic deformation occurs at higher levels of deformation. However, the plastic deformation has a stronger effect on the fatigue life for fine pearlite. For one same plastic deformation, CP resists to more cycles than FP. This may indicate that coarse pearlite is more resistant in fatigue than fine pearlite when this method is taken into consideration.

One other common approach to the study of fatigue behaviour is the stress-life approach (S-N), in which the stress is imposed and the effects in the strain behaviour of the material are observed [18]. In a complementary study [27], the same samples (CP and FP) were subjected to fatigue tests using the S-N approach. The results showed that, during cycling at constant stress, the values of total strain and the plastic strain observed in the hysteresis curves increased as the material was cycled. For the same stress, an increase in strain was

noticed. This result can also be interpreted as a softening of the material, confirming that both the ε-N approach and the S-N approach resulted in the same behaviour, and thus both methods are similar and comparable in terms of material response.

SEM images of the fracture surface showed three different behaviours: the first observed for CP at 1.2% and 1.6% of total deformation and FP at 1.6%, 1.2% and 0.8% of total deformation, with an unstable final fracture by cleavage and ductile transition zone; the second for CP at 0.6% and 0.8% of total deformation, with a brittle transition zone and final ductile fracture and the third, for FP at 0.6% of total deformation, with no transition zone and a final ductile fracture. All the fracture surfaces started by microplastic tearing.

The observation of the microplastic tearing in the fatigue propagation of the crack in a stable mode is in agreement with the literature [19-23]. Toribio et al. [21] attributed this behaviour of accumulation of localized plastic deformation in the lamellar structure. Also, the surface does not have striations marks. One proposed mechanism was the shear crack of the pearlite by the fracture of the cementite lamella after the plastic deformation of the matrix ferrite. The final fracture by cleavage was also observed by Toribio et al. [23], due to the unstable propagation of the crack. The brittle fracture may have occurred in the pearlite colonies. To prove this theory, measurements of the colony side should be done and compared to the patterns of rivers marks.

The images of the relief marks agree with the data from the hysteresis curves. Higher levels of deformation generate higher plastic deformation. In addition, coarse pearlite showed more plastic deformation than fine for all levels of deformations. As a result, more intrusion/extrusion couples were observed for higher levels of deformation and coarse pearlite when compared to the fine pearlite at the same level of deflation. This relation was expected from the literature [18].

Coarse and fine pearlite show similar small cracks propagation profiles. Those cracks are originated from the intrusion/extrusion couples but did not propagate enough to cause the rupture. In both cases, the crack propagated in a transgranular direction, regarding the pearlite colonies. Ravichandran [16] says that both transgranular and intergranular directions are possible in pearlitic steels,

but the behaviour is highly affected by the pearlite colony size. Hence, further analysis of this microstructural characteristic of the materials must be analyzed.

6. Conclusions

In this study, fatigue tests were performed controlling the values of total deformation for two samples: fine pearlite (FP) and coarse pearlite (CP). The samples were subjected to total deformations of 0.6%, 0.8%, 1.2% and 1.6%, always in traction. Complementarily, images of the fracture surface, surface topography and small crack propagation were taken using the scanning electron microscopy. The main conclusions of this study are:

1. Finer pearlite is harder and presents a higher Young's modulus than coarse pearlite. CP deformed more plastically during cycling. Both samples showed softening and the relaxation effect during cycling. Thus, increasing the interlamellar spacing reduces the number of interfaces, and those effects are reduced.
2. The strain life curve showed that coarse pearlite could accommodate a higher plastic deformation without failing. This may indicate that this material has a better fatigue resistance than fine pearlite, as the plastic deformation is an indicator of damage.
3. Fractographies of fine pearlite samples (total deformation of 0.8%, 1.2% and 1.6%) and coarse pearlite (total deformation of 1.2% and 1.6%) showed to plane zones: a smoother related to the stable crack propagation of the fatigue crack featuring microplastic coalescence and presence of small secondary cracks. The second zone is the unstable crack propagation due to mechanical overload, featuring rivers marks and cleavage. Dimples were found in the interface of both regions.
4. In the fractographies of the coarse pearlite samples (total deformation of 0.6% and 0.8%) the same initial stable crack propagation was observed, but the crack propagation by overload was ductile, with a transition area featuring rivers marks. The fracture surface for the fine pearlite samples (total deformation of 0.6%) was similar to CP at small values of total deformations but without the presence of unstable crack propagation zone with the rivers marks.
5. Surface topography images confirmed the results of the fatigue tests. Coarse pearlite that showed more plastic deformation during cycling presented more prominent and more numerous intrusions and extrusions marks.

6. In both coarse and fine pearlite, the crack seems to propagate in a transgranular direction, crossing the pearlite colonies.

7. References

[1] RUSSO, Francesco M. et al. **Design and Evaluation of Steel Bridges for Fatigue and Fracture–Reference Manual**. National Highway Institute (US), 2016.

[2] PERELOMA, Elena; EDMONDS, David V. (Ed.). **Phase transformations in steels: fundamentals and diffusion-controlled transformations**. Elsevier, 2012.

[3] SHIMOKAWA, Tomotsugu et al. Interfacial-dislocation-controlled deformation and fracture in nanolayered composites: toward higher ductility of drawn pearlite. **Acta Materialia**, v. 164, p. 602-617, 2019.

[4] SORBY, Henry Clifton. On microscopical photographs of various kinds of iron and steel. **British Association Report, Part II**, p. 189, 1864.

[5] CARPENTER, H. C. H.; ROBERTSON, J. M. The austenite-pearlite inversion. **J. Iron Steel Inst. London**, v. 125, p. 309, 1932.

[6] MEHL, Robert F.; HAGEL, William C. The austenite: pearlite reaction. **Progress in Metal Physics**, v. 6, p. 74-134, 1956.

[7] KRAUSS, George. **Steels: processing, structure, and performance**. Asm International, 2015.

[8] ELWAZRI, A. M.; YUE, S.; WANJARA, P. Effect of prior-austenite grain size and transformation temperature on nodule size of microalloyed hypereutectoid steels. **Metallurgical and Materials Transactions A**, v. 36, n. 9, p. 2297, 2005.

[9] ZHANG, Fei et al. Study on the Nucleation and Growth of Pearlite Colony and Impact Toughness of Eutectoid Steel. **Metals**, v. 9, n. 11, p. 1133, 2019.

[10] HAMADA, S. et al. Fatigue limit evaluation considering crack initiation for lamellar pearlitic steel. **Procedia Engineering**, v. 10, p. 1467-1472, 2011.

[11] NAM, Won Jong; BAE, Chul Min; LEE, Chong Soo. Effect of carbon content on the Hall-Petch parameter in cold drawn pearlitic steel wires. **Journal of materials science**, v. 37, n. 11, p. 2243-2249, 2002.

[12] HALL, E. O. The deformation and ageing of mild steel: III discussion of results. **Proceedings of the Physical Society. Section B**, v. 64, n. 9, p. 747, 1951.

[13] PETCH, N. J. The cleavage strength of polycrystals. **Journal of the Iron and Steel Institute**, v. 174, p. 25-28, 1953.

[14] NAIK, Sneha N.; WALLEY, Stephen M. The Hall–Petch and inverse Hall–Petch relations and the hardness of nanocrystalline metals. **Journal of Materials Science**, v. 55, n. 7, p. 2661-2681, 2020.

[15] CORDERO, Zachary C.; KNIGHT, Braden E.; SCHUH, Christopher A. Six decades of the Hall–Petch effect–a survey of grain-size strengthening studies on pure metals. **International Materials Reviews**, v. 61, n. 8, p. 495-512, 2016.

[16] RAVICHANDRAN, K. S. A rationalization of fatigue thresholds in pearlitic steels using a theoretical model. **Acta metallurgica et materialia**, v. 39, n. 6, p. 1331-1341, 1991.

[17] LAMPMAN, Steven R. ASM handbook: Volume 19, fatigue and fracture. **ASM International**, 1996.

[18] STEPHENS, Ralph I. et al. **Metal fatigue in engineering**. John Wiley & Sons, 2000.

[19] TORIBIO, Jesús; GONZÁLEZ, Beatriz; MATOS, Juan-Carlos. Analysis of fatigue crack paths in cold drawn pearlitic steel. **Materials**, v. 8, n. 11, p. 7439-7446, 2015.

[20] MAYA-JOHNSON, S.; RAMIREZ, A. J.; TORO, A. Fatigue crack growth rate of two pearlitic rail steels. **Engineering fracture mechanics**, v. 138, p. 63-72, 2015.

[21] TORIBIO, J.; MATOS, J. C.; GONZÁLEZ, B. Micro-and macro-approach to the fatigue crack growth in progressively drawn pearlitic steels at different R-ratios. **International Journal of Fatigue**, v. 31, n. 11-12, p. 2014-2021, 2009.

[22] GRAY, G. T.; THOMPSON, A. W.; WILLIAMS, J. C. Influence of microstructure on fatigue crack initiation in fully pearlitic steels. **Metallurgical Transactions A**, v. 16, n. 5, p. 753-760, 1985.

[23] TORIBIO, J.; GONZÁLEZ, B.; MATOS, J. C. Crack paths in cold drawn pearlitic steel subjected to fatigue and fracture. **CP2009**, 2013.

[24] TORIBIO, J. et al. Multi-Scale Approach to the Fatigue Crack Propagation in High-Strength Pearlitic Steel Wires. **Journal of ASTM International**, v. 5, n. 6, p. 1-15, 2008.

[25] Personal conversation – Isadora M. O. A. Costa – Mail Exchange – 16/07/2019

[26] D'ÁVILA, DÓRIS CORSI RIBAS. INFLUÊNCIA DO ESPAÇAMENTO INTERLAMELAR NO COMPORTAMENTO EM FADIGA DE FIOS DE AÇOS PERLÍTICOS. TCC, EPUSP, 2020. ResearchGate.

[27] AIRES, Ana B. B. L., DOLABELLA, Ana C. A., SARTORI, Guilherme A. C. FATIGUE OF PEARLITIC STEELS USED FOR BRIDGE CABLES

Appendix A - Graphics from the fatigue testing

Cyclic accommodation curves as a function of the number of cycles in logarithmic scale:

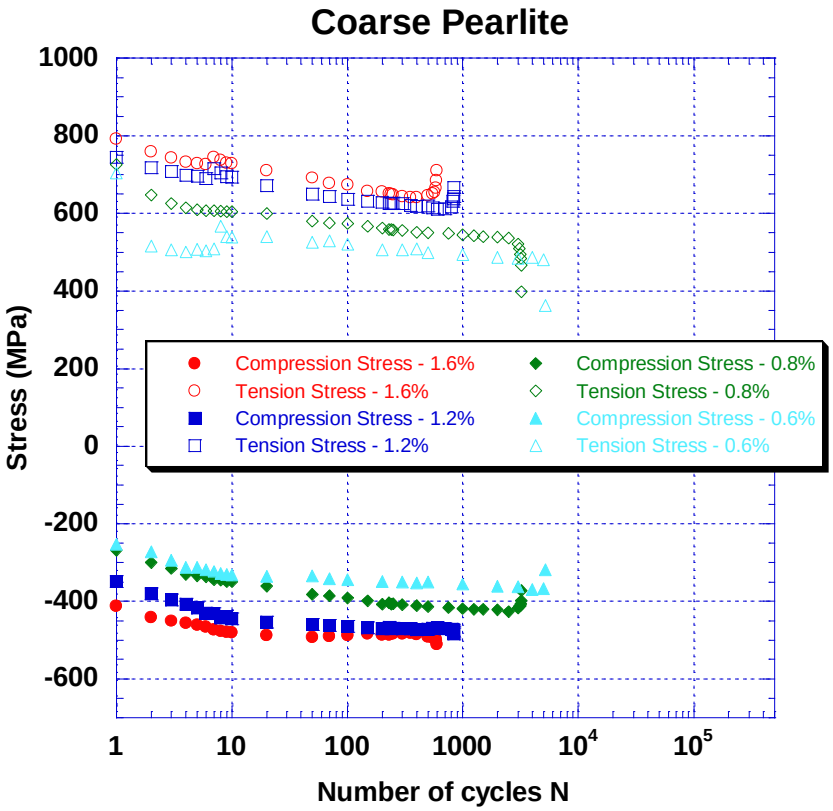

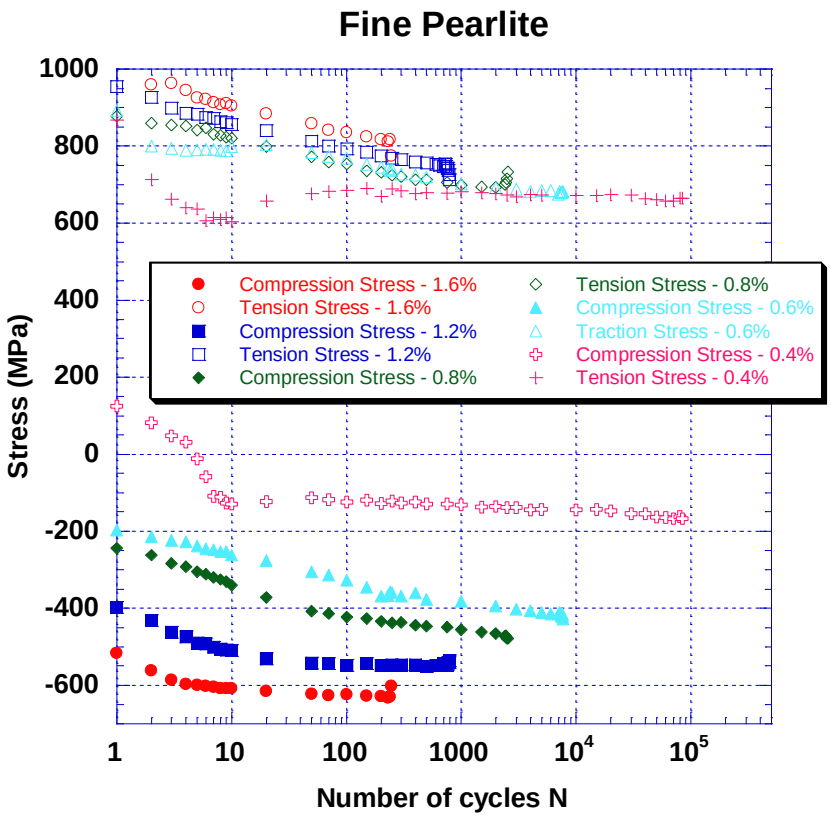

Observation: for fine pearlite, tests at 0.4% were carried out, but the results were not conclusive and thus were not discussed on this project.

Cyclic accommodation curves as a function of the fatigue life fraction in linear scale:

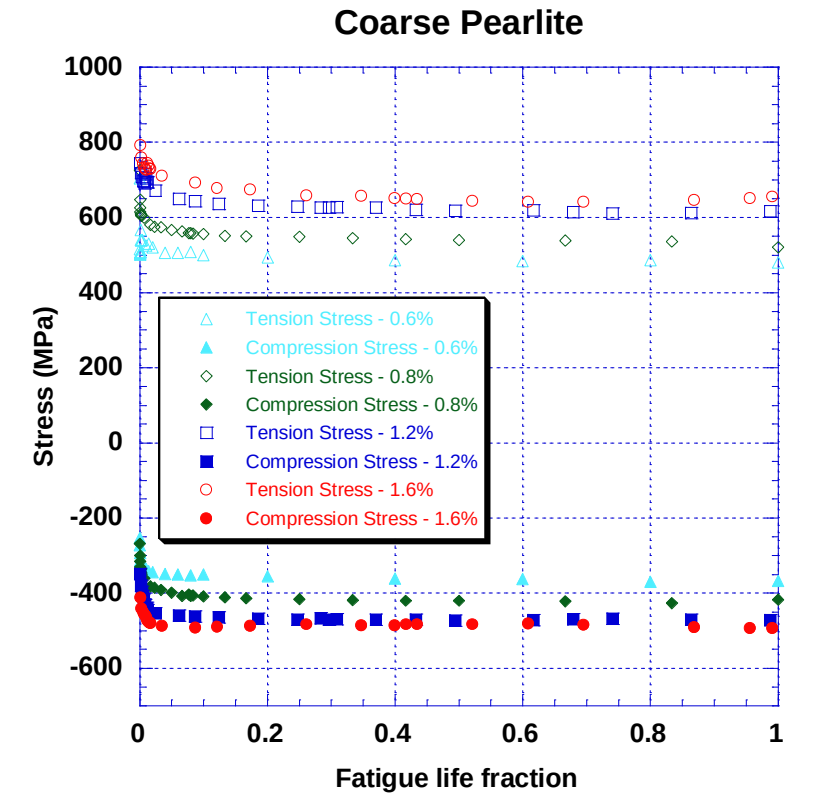

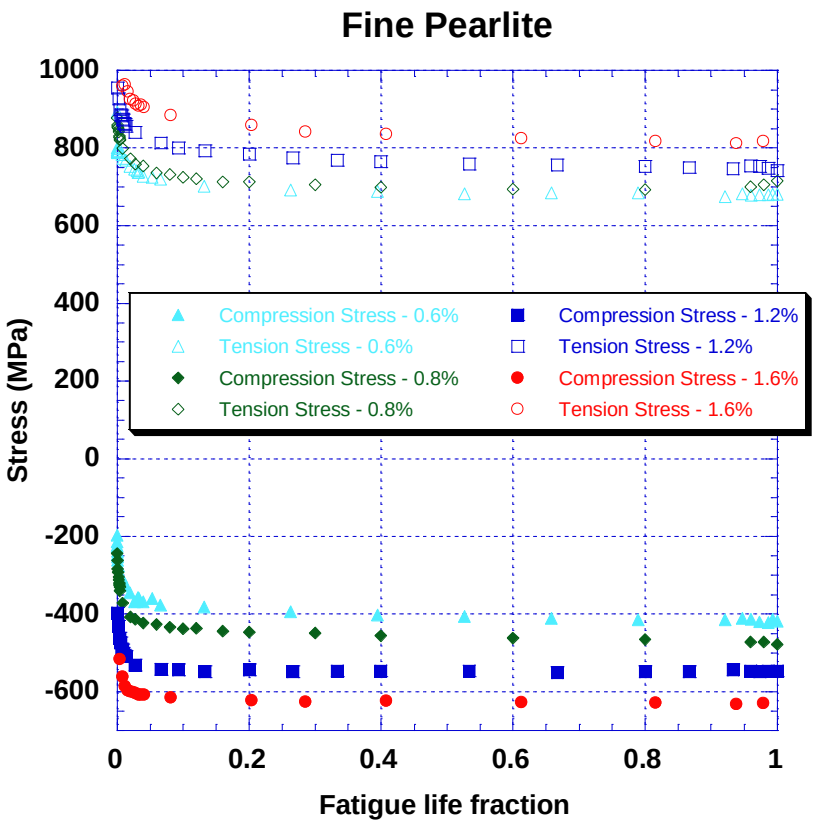

All hysteresis curves for all the levels of deformation in the half-life of fatigue:

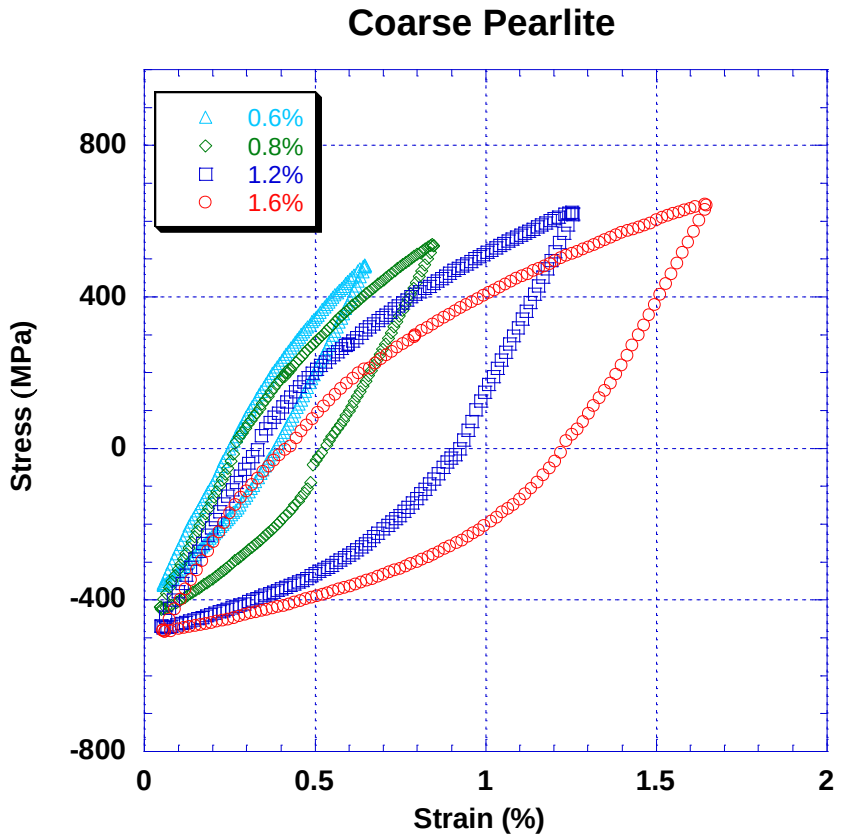

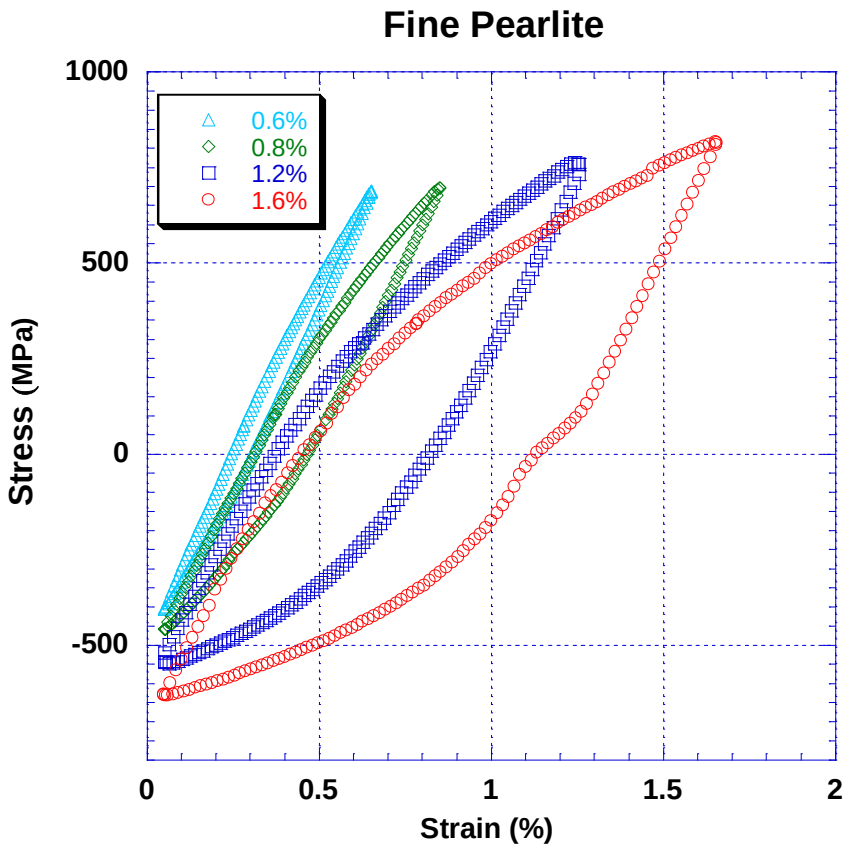

Appendix B – SEM images of the fracture surface

For FP, 0.6% of total deformation:

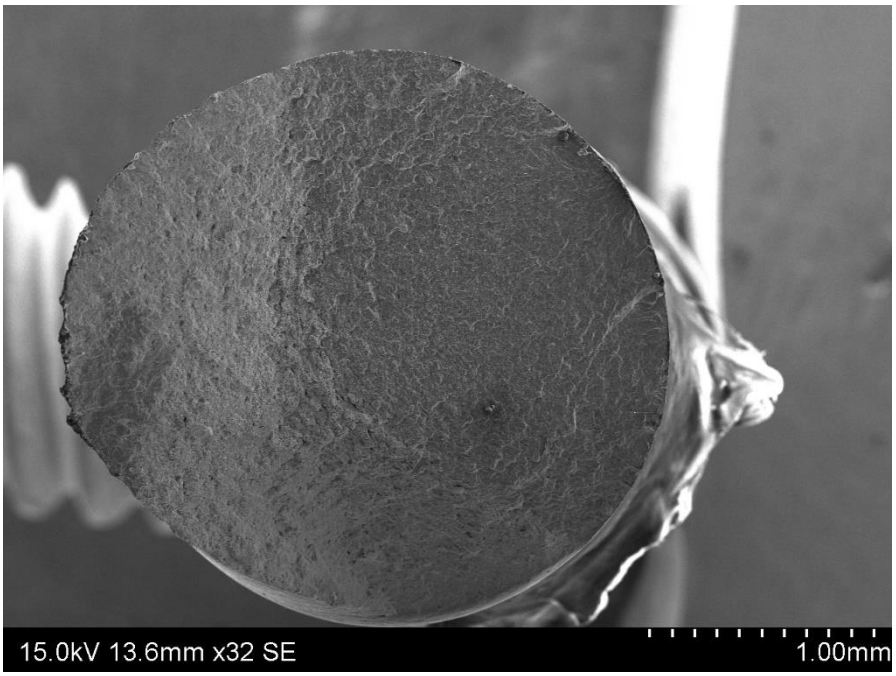

For FP, 0.8% of total deformation:

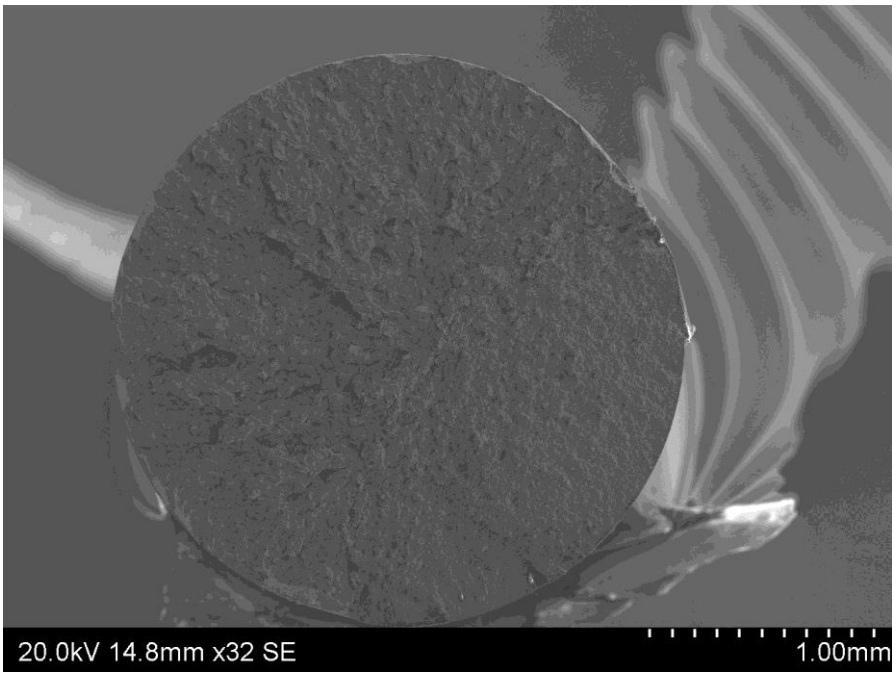

For FP, 1.2% of total deformation:

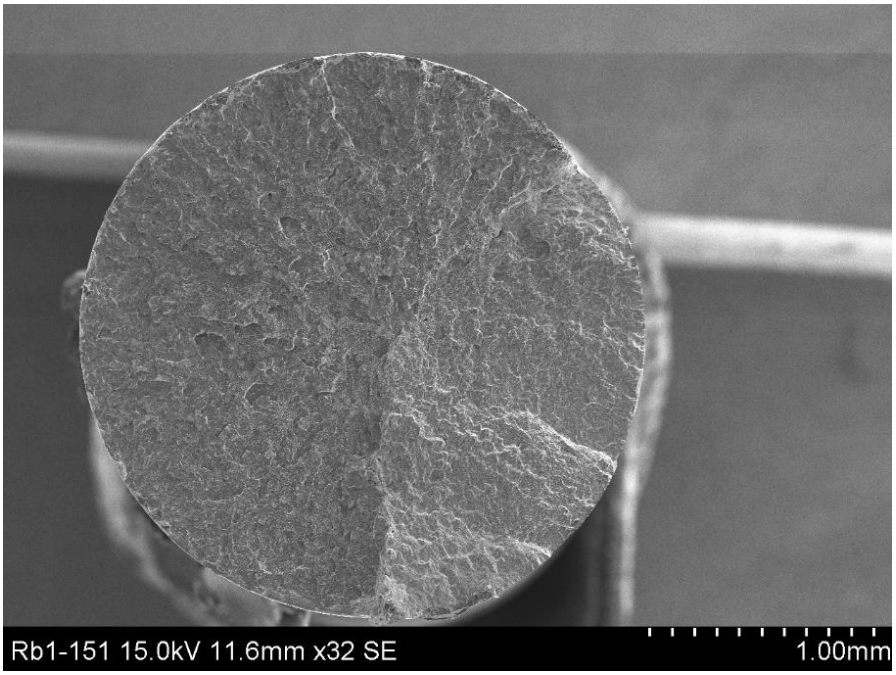

For FP, 1.6% of total deformation:

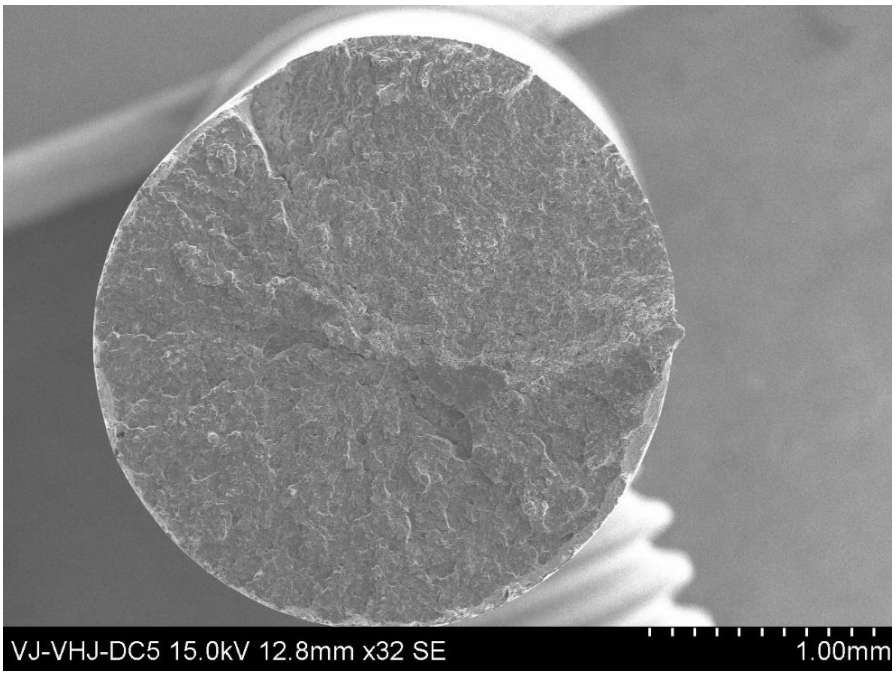

For CP, 0.6% of total deformation:

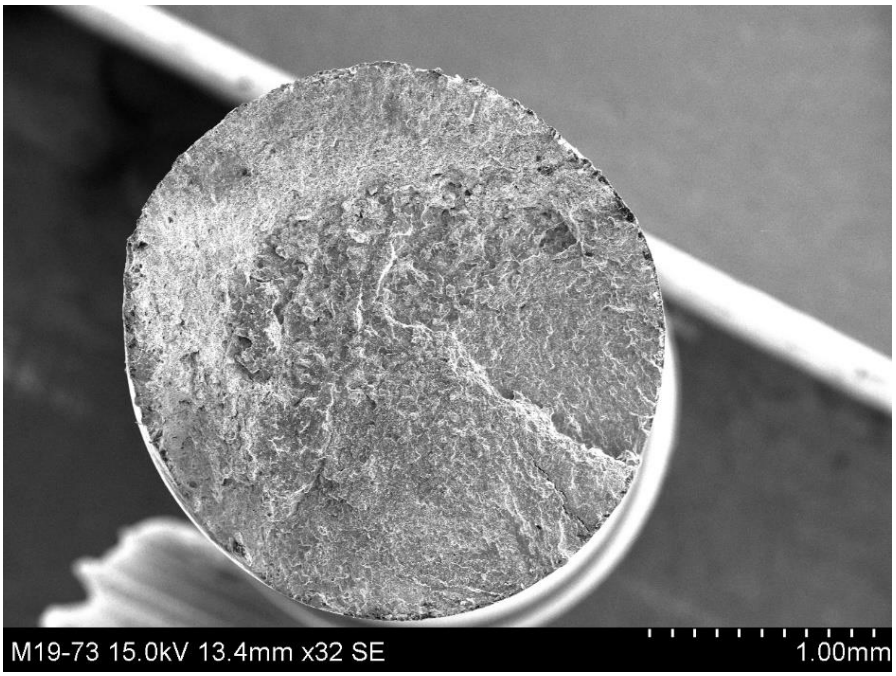

For CP, 0.8% of total deformation:

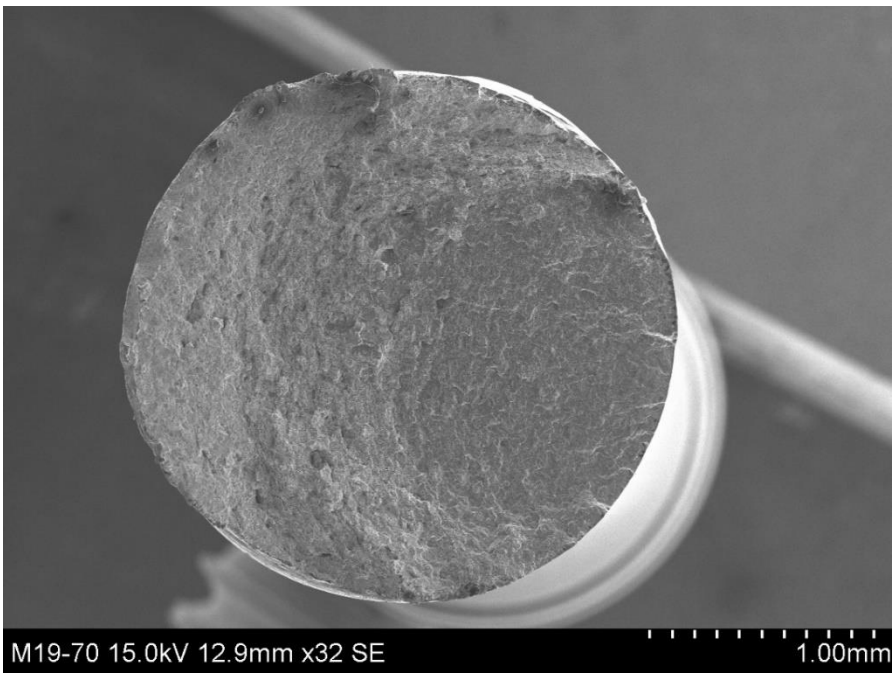

For CP 1.2% of total deformation:

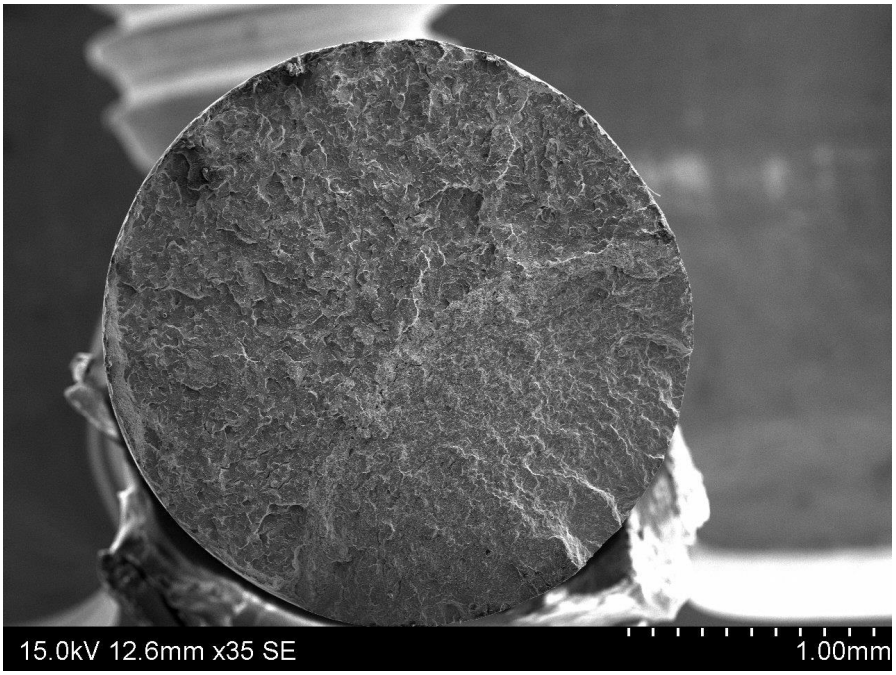

For CP 1.6% of total deformation: